Project Number 282910

ÉCLAIRE

Effects of Climate Change on Air Pollution Impacts and Response Strategies for European Ecosystems

Seventh Framework Programme

Theme: Environment

D1.6 Publications from the integrated campaign at Bosco Fontana

Due date of deliverable: **01/04/2015** Actual submission date: **30/09/2015**

Start Date of Project: **01/10/2011** Duration: **48 months**

Organisation name of lead contractor for this deliverable : **NERC**

Project co-funded by the European Commission within the Seventh Framework Programme		
Dissemination Level		
PU	Public	X
PP	Restricted to other programme participants (including the Commission Services)	☐
RE	Restricted to a group specified by the consortium (including the Commission Services)	☐
CO	Confidential, only for members of the consortium (including the Commission Services)	☐

1. Executive Summary:

Four papers have been drafted reporting the results for publication in open-access ISI listed peer reviewed journals, namely *Atmospheric Chemistry and Physics* as well as *Biogeosciences*:

1. Acton, W. J. F., Schallhart, S., Langford, B., Valach, A., Rantala, P., Fares, S., Carriero, G., Tillmann, R., Tomlinson, S. J., Dragosits, U., Gianelle, D., Hewitt, C. N., and Nemitz, E.: Canopy-scale flux measurements and bottom-up emission estimates of volatile organic compounds from a mixed oak and hornbeam forest in northern Italy, Atmos. Chem. Phys. Discuss., 15, 29213-29264, doi:10.5194/acpd-15-29213-2015, 2015.

2. Schallhart, S., Rantala, P., Nemitz, E., Mogensen, D., Tillmann, R., Mentel, T. F., Rinne, J., and Ruuskanen, T. M.: Characterization of total ecosystem scale biogenic VOC exchange at a Mediterranean oak-hornbeam forest, Atmos. Chem. Phys. Discuss., 15, 27627-27673, doi:10.5194/acpd-15-27627-2015, 2015.

3. Twigg, M.M., Di Marco, C.F., Langford, B., Loubet, B., Gerosa, G., Finco, A., Sutton, M.A., Nemitz, E.: Controls of reactive nitrogen fluxes and gas-aerosol interactions above a semi-natural forest in the Po Valley, Italy. Atmos. Chem. Phys. Discuss. [in preparation]

4. Finco, A., Coyle, M.; Marzuoli, R.; Chiesa, M.; Loubet, B.; Diaz-Pines, E.; Gasche, R.; Ammann, C.; Sutton, M.A.; Nemitz, E., Gerosa, G.: Ozone fluxes measurements at four levels above, inside and below a forest canopy: interactions with nitrous oxide and implications for the ozone flux partition. Biogeosciences Discuss. [in preparation]

2. Abstract of Paper #1 “Canopy-scale flux measurements and bottom-up emission estimates of volatile organic compounds from a mixed oak and hornbeam forest in northern Italy”

(full text can be found at: http://www.atmos-chem-phys-discuss.net/15/29213/2015/acpd-15-29213-2015.html)

This paper reports the fluxes and mixing ratios of biogenically emitted volatile organic compounds (BVOCs) 4 m above a mixed oak and hornbeam forest in northern Italy. Fluxes of methanol, acetaldehyde, isoprene, methyl vinyl ketone + methacrolein, methyl ethyl ketone and monoterpenes were obtained using both a proton transfer reaction-mass spectrometer (PTR-MS) and a proton transfer reaction-time of flight-mass spectrometer (PTR-ToF-MS) together with the methods of virtual disjunct eddy covariance (PTR-MS) and eddy covariance (PTR-ToF-MS). Isoprene was the dominant emitted compound with a mean day-time flux of 1.9 mg m^{-2} h^{-1}. Mixing ratios, recorded 4 m above the canopy, were dominated by methanol with a mean value of 6.2 ppbv over the 28 day measurement period. Comparison of isoprene fluxes calculated using the PTR-MS and PTR-ToF-MS showed very good agreement while comparison of the monoterpene fluxes suggested a slight over estimation of the flux by the PTR-MS. A basal isoprene emission rate for the forest of 1.7 mg m^{-2} h^{-1} was calculated using the MEGAN isoprene emissions algorithms (Guenther et al., 2006). A detailed tree species distribution map for the site enabled the leaf-level emissions of isoprene and monoterpenes recorded using GC-MS to be scaled up to produce a "bottom-up" canopy-scale flux. This was compared with the "top-down" canopy-scale flux obtained by measurements. For monoterpenes, the two estimates were closely correlated and this correlation improved when the plant species composition in the individual flux footprint was taken into account. However, the bottom-up approach significantly underestimated the isoprene flux, compared with the top-down measurements, suggesting that the leaf-level measurements were not representative of actual emission rates.

3. Abstract of Paper #2 "Characterization of total ecosystem scale biogenic VOC exchange at a Mediterranean oak-hornbeam forest"

(Full text can be found at: http://www.atmos-chem-phys-discuss.net/15/27627/2015/acpd-15-27627-2015.html)

Recently, the number and amount of biogenically emitted volatile organic compounds (VOCs) has been discussed vigorously. Depending on the ecosystem the published number varies between a dozen and several hundred compounds. We present ecosystem exchange fluxes from a mixed oak-hornbeam forest in the Po Valley, Italy. The fluxes were measured by a proton transfer reaction-time-of-flight (PTR-ToF) mass spectrometer and calculated by the eddy covariance (EC) method. Detectable fluxes were observed for twelve compounds, dominated by isoprene, which comprised over 65 % of the total flux emission. The daily average of the total VOC emission was 9.5 nmol m^{-2} s^{-1}. Methanol had the highest concentration and accounted for the largest deposition. Methanol seemed to be deposited to dew, as the deposition happened in the early morning, right after the calculated surface temperature came closest to the calculated dew point temperature.

We estimated that up to 27 % of the upward flux of methyl vinyl ketone (MVK) and methacrolein (MACR) originated from atmospheric oxidation of isoprene. A comparison between two flux detection methods (classical/visual and automated) was made. Their respective advantages and disadvantages were discussed and the differences in their results shown. Both provide comparable results; however we recommend the automated method with a compound filter, which combines the fast analysis and better flux detection, without the overestimation due to double counting.

4. Abstract of paper #3 "Controls of reactive nitrogen fluxes and gas-aerosol interactions above a semi-natural forest in the Po Valley, Italy."

(full draft below)

A comprehensive international measurement campaign was conducted in summer 2012 to investigate the interaction between emission / deposition, chemistry and transport of N compounds above an oak-hornbeam forest "Bosco Fontana" near Mantova, situated in the Po Valley, Italy. The focus of this paper is to investigate the magnitude and controls of the dry deposition of reactive N compounds. In addition, within plant canopies, turbulent transport is slow and the gradients of concentrations and meteorological parameters (radiation, temperature, humidity) are often steep. This results in chemical sources and sinks for reactive trace compounds. As a result, flux measurements above the vegetation may deviate from the true biosphere-atmosphere exchange. We here present fluxes obtained by eddy-covariance using an aerosol mass spectrometer (sub-micron NH_4^+ and NO_3^-), and with a wet chemistry gradient system, GRAEGOR, which measured water soluble aerosols (NH_4^+, Cl^-, NO_3^- and SO_4^{2-}) and their counterpart gas phase species (NH_3, HCl, HNO_3 and SO_2) to derive fluxes at a 1 hour resolution at the top of a forest using both a modified aerodynamic gradient approach and inferential modelled flux. The average concentrations above the forest canopy (41 m) were 30.43 µg m^{-3}, 2.55 µg m^{-3}, 0.68 µg m^{-3}, 3.10 µg m^{-3}, 4.95 µg m^{-3}, for NH_3, HNO_3, HONO, NH_4^+ and NO_3^- respectively. The largest flux was NH_3 with an average deposition flux of -253.42 ng m^{-2} s^{-1}, whereas expected HNO_3 had the greatest average V_d of 18.80 mm s^{-1} of the N compounds measured. Apparent aerosol deposition rates of NH_4^+ and NO_3^- were greatly enhanced during the day due to evaporation during the deposition process near the surface where the gas-aerosol partitioning was skewed towards the aerosol phase compared with equilibrium calculations. At the same time the measured HNO_3 deposition rate was reduced.

The average dry N deposition during the campaign was 237 ng N m^{-2} s^{-1}, with the largest N input from NH_3 (75%), followed by the aerosol components (jointly 19%) and HNO_3 (5%). This equates to an inferred annual total of almost 75 kg N ha^{-1} yr^{-1}, bravely extrapolated from 2 weeks' of summer measurements, which would exceed the N throughfall deposition previously reported for the same site.

5. Abstract of paper #4 “Ozone fluxes measurements at four levels above, inside and below a forest canopy: interactions with nitrous oxide and implications for the ozone flux partition.”

(full draft below)

Ozone is detrimental to plants and human health. It is therefore important to develop a robust understanding of how efficiently ozone is deposited to vegetation and to identify the fraction of ozone that enters the stomata where it can cause phytotoxic damage. As part of the FP7 ECLAIRE project an integrated field campaign at the hornbeam-oak forest at Bosco Fontana, Po Valley, Italy, brought together sufficient instrumentation to attribute the O_3 flux to the different pathways. Ozone fluxes were measured at four heights above, within and below the crown space, whilst fluxes of NO were determined at the ground and above the canopy. The O_3 deposition were typically 10 nmol m^{-2} s^{-1} during the day and 2 nmol m^{-2} s^{-1} at night. Soil NO emissions showed little diurnal variability and averaged 76.8 ng N m^{-2} s^{-1}. The detailed results suggest that about 40% of the ozone flux enters the stomata and 30% reacts with NO, based on the difference in the NO flux from the soil and above the canopy. With only 35% of the flux removed by the crown space, it follows that (a) there are stomatal sinks in the understorey, (b) cuticular O_3 deposition in the crown space is insignificant and (c) reaction with NO occurs mainly below the crown layer. The measurements further shed light on the interaction between in-canopy inversion and O_3 exchange.

Controls of reactive nitrogen fluxes and gas-aerosol interactions above a semi-natural forest in the Po Valley, Italy.

Twigg, M.M.[1] Di Marco, C.F. [1] Langford, B. [1] Loubet, B.[2] Gerosa, G.[3] Finco, A.[3] Sutton, M.A.[1] Nemitz, E.[1]

[1] NERC Centre for Ecology and Hydrology (CEH), Bush Estate, Penicuik, EH26 0QB, UK.

[2] INRA, UMR 1091-INRA-AgroParisTech, Environnement et Grandes Cultures, 78850 Thiverval-Grignon, France

[3] Dip. to di Matematica e Fisica, Università Cattolica del S.C., via Musei 41, 25121 Brescia, Italy

Correspondence to: M. M. Twigg (sail@ceh.ac.uk)

Abstract

A comprehensive international measurement campaign was conducted in summer 2012 to investigate the interaction between emission / deposition, chemistry and transport of N compounds above an oak-hornbeam forest “Bosco Fontana” near Mantova, situated in the Po Valley, Italy. The focus of this paper is to investigate the magnitude and controls of the dry deposition of reactive N compounds. In addition, within plant canopies, turbulent transport is slow and the gradients of concentrations and meteorological parameters (radiation, temperature, humidity) are often steep. This results in chemical sources and sinks for reactive trace compounds. As a result, flux measurements above the vegetation may deviate from the true biosphere-atmosphere exchange. We here present fluxes obtained by eddy-covariance using an aerosol mass spectrometer (sub-micron NH_4^+ and NO_3^-), and with a wet chemistry gradient system, GRAEGOR, which measured water soluble aerosols (NH_4^+, Cl^-, NO_3^- and SO_4^{2-}) and their counterpart gas phase species (NH_3, HCl, HNO_3 and SO_2) to derive fluxes at a 1 hour resolution at the top of a forest using both a modified aerodynamic gradient approach and inferential modelled flux. The average concentrations above the forest canopy (41 m) were 30.43 µg m^{-3}, 2.55 µg m^{-3}, 0.68 µg m-3, 3.10 µg m^{-3}, 4.95 µg m^{-3}, for NH_3, HNO_3, HONO, NH_4^+ and NO_3^- respectively. The largest flux was NH_3 with an average deposition flux of -253.42 ng m^{-2} s^{-1}, whereas expected HNO_3 had the greatest average V_d of 18.80 mm s^{-1} of the N compounds measured. Apparent aerosol deposition rates of NH_4^+ and NO_3^- were greatly enhanced during the day due to evaporation during the deposition process near the surface where the gas-aerosol partitioning was skewed towards the aerosol phase compared with equilibrium calculations. At the same time the measured HNO_3 deposition rate was reduced.

The average dry N deposition during the campaign was 237 ng N m^{-2} s^{-1}, with the largest N input from NH_3 (75%), followed by the aerosol components (jointly 19%) and HNO_3 (5%). This equates to an

inferred annual total of almost 75 kg N ha^{-1} yr^{-1}, bravely extrapolated from 2 weeks' of summer measurements, which would exceed the N throughfall deposition previously reported for the same site.

1 Introduction

Atmospheric reactive inorganic compounds of nitrogen in gas and aerosol phase have a multitude of environmental impacts. Ammonia (NH_3) is the primary alkaline gas in the troposphere, often dominates the atmospheric dry deposition of reactive nitrogen, and its deposition is well documented to cause eutrophication and acidification of ecosystems, as well as indirectly impacting both the climate and human health through the formation of secondary inorganic aerosols (Sutton et al., 2009). Since the reduction of sulphur dioxide (SO_2) over the last 30 years in Western Europe, nitric acid (HNO_3) has become important precursor of secondary inorganic aerosols through the interaction with NH_3. Recent research demonstrated the dominance of nitrate (NO_3^-) as a secondary inorganic aerosol (Fowler et al., 2015) in Western Europe. In Europe an important combined 'hot spot' for emissions of NH_3 and NO_x, the precursors of HNO_3, is in the Po Valley in Northern Italy, reflecting a combination of intensive agriculture and industry. This region is a flood plain surrounded by the Alps in the Western and Northern side, Apennines on Southern side and the Adriatic Sea to the East. The population within the Po Valley is estimated to be 20 million (Zhu et al., 2012) and is a region of intensive agriculture and industry in Europe, contributing 50% to the total Italian GDP (Zhu et al., 2012). The scale of the NH_3 'hot spot' of the Po Valley in Europe has been demonstrated by satellite studies deriving total NH_3 column concentrations (Van Damme et al., 2014). The 'hot spot' observed was attributed by Van Damme et al. (2014) to be the result of both intensive agriculture and the topography of the region. Due to the Po Valleys poor air quality, a number of studies have been carried out to understand the atmospheric composition and tropospheric chemistry in the region (Decesari et al., 2014;Decesari et al., 2001;Matta et al., 2003;Bigi et al., 2012;Mélin and Zibordi, 2005).

Yet, even though emissions of NH_3 and NO_x are high in the Po Valley, there are limited studies on dry deposition of reactive N to the local ecosystems, with previous studies inferring deposition based on long-term concentration measurements of reactive N species by throughfall methods to forests (Ferretti et al., 2014). The reason for the lack of direct flux measurements is the result of the difficulty of measuring reactive N species such as NH_3 and HNO_3 due to their 'sticky' and reactive nature. Over the last two decades there has been a rapid development in the technology available to measure fluxes for NH_3 and trace acidic species (HNO_3 and HONO) including wet chemistry instruments such as the MARGA (monitor for aerosols and gases in ambient air, Metrohm-Applikon, NL) (Makkonen et al., 2012;Rumsey et al., 2014;Twigg et al., 2015) and the GRAEGOR (gradient of aerosol and gases online registrator; ECN, Petten, NL) (Thomas et al., 2009;Trebs et al., 2004;Wolff et al., 2010). The

disadvantage of using a wet chemistry method is there is the potential for artefacts in the measurement, for example N_2O_5 converts to NO_3^- in H_2O and therefore would be reported as HNO_3 (Phillips et al., 2013). There is an additional wet chemistry method, the LOPAP (long path absorption spectrometer), which is thought to be a largely artefact free chemistry method for HONO (Kleffmann et al., 2005) and has recently been applied to measure fluxes in the field (Sörgel et al., 2015). Other techniques such as mass spectrometry have also been used to measure trace N species including the use of the CIMS (chemical ionisation mass spectrometer) for NH_3 fluxes (Sintermann et al., 2011). The final set of instrumentation use absorption spectrometry, historically methods include photoacoustic systems for NH_3 (Pogány et al., 2010), TDLs (tunable diode lasers) specifically for NH_3 and HNO_3 (Twigg et al., 2011;Whitehead et al., 2008;Volpe Horii et al., 2005) or more recently commercial QCL (quantum cascade lasers) systems, though there is currently very limited literature on their application of fluxes for reactive N trace species such as NH_3 (Ferrara et al., 2012). The problem with both the mass spectrometry and absorption spectrometry methods there is a need for fast resolution measurements (>1 Hz) and a fairly long inlet (>1 m) in order to measure the fluxes by eddy covariance but due to the sticky and reactive nature of the species of interest there are problems in interferences due to cell wall interactions. There are currently developments in trying to limit wall interactions for inlets for reactive N species such as passivated sampling, though this method is in its infancy (Roscioli et al., 2015).

As well as challenges with instrumentation, there are also micrometeorological challenges when measuring fluxes over tall vegetation (see Section 3.3 for discussion). As a result, measurements of NH_3 fluxes and other reactive N species over deciduous forests are particularly limited in the literature as previous work has tended to focus on short vegetation such as grasslands, where the complexities in measuring the conserved flux are reduced (Sintermann et al., 2011;Trebs et al., 2004;Twigg et al., 2011). There are also additional chemical complexities in quantifying NH_3 and HNO_3 over forests, as studies have demonstrated that the flux may not be conserved near a canopy due to gas-aerosol partitioning of ammonium nitrate (Nemitz et al., 2004a, b; Nemitz and Sutton, 2004; Wolff et al., 2010). As a result of a non-conserved flux the NH_3 deposition flux can either be overestimated due to aerosol formation or underestimated, with potentially the direction of the flux reversed due to volatilisation of NH_4NO_3 close to the canopy. Wolff et al. (2010) is one of the only studies in literature which has investigated the NH_3-HNO_3-NH_4NO_3 triad over a forest canopy.

The present work forms part of an integrated European funded study (Effects of Climate Change on Air Pollution and Response Strategies for European Ecosystems (ÉCLAIRE), EU FP7) to assess the in-canopy chemistry effect on the fluxes of NO-NO_2-O_3–VOC and NH_3-HNO_3-aerosol over a forest in the Po Valley, Italy during June-July 2012. As part of this study concentrations and fluxes were measured of NH_3, HNO_3, HONO, HCl, SO_2 and their counterpart aerosols (NH_4^+, NO_3^-,Cl^-, SO_4^{2-}) by a GRAEGOR instrument. This investigation focuses on the N fluxes measured by the GRAEGOR instrument, but

presents other species measured. The aim of this work is to establish the importance of individual N species to the dry deposition budget in the Po Valley.

The O_3, NOx and VOC measurements during this campaign have been presented elsewhere (Finco et al., 2015; Schallhart et al., 2015; Acton et al., 2015).

2 Methods

2.1 Field site description

Bosco Fontana nature reserve is situated north of Mantova in the Po valley, Italy (45° 11' 51" N, 10° 44' 31" E) at 30 m above sea level. The forest covers 233 ha which is dominated by four broadleaf species (*Carpinus betulus, Quercus robur, Quercus rubra and Qucerus cerris*) (Dalponte et al., 2008) with an average canopy height of ~ 28m. A "dead wood" management system is used at Bosco Fontana for ~ last 20 years, where all the fallen trees are left where they fall in order to increase the biodiversity from the microbial scale to the ecosystem level. The non-native *Q. Rubra* is gradually removed from the forest by pulling down tress and leaving them. The measurement campaign took place from the 1st June 2012 to 11th July 2012, though data reported here was from 27th June 2012 to 10th July 2012 when the GRAEGOR was operated in flux mode. The dominant wind direction during whole the field campaign was from an easterly direction (Acton et al., 2015), though the period presented here was dominated by a W-NW direction.

2.2 Instrumentation

Table 1 provides a summary of the instrumentation used in the measurements of trace gases, aerosols and micrometeorological parameters at the field site, the setup of which is illustrated in Fig. 1. Further results from this campaign are described elsewhere (Finco et al., In preperation;Acton et al., 2015).

Table 1 summary of instrumentation used during the Bosco Fontana Campaign

Instrument	Parameter measured	Reporting Resolution	Measurement Height	Flux technique
GRAEGOR	Gases: NH_3, HNO_3, HONO, HCl, SO_2 Aerosol: NO_3^-, Cl^-, SO_4^{2-}, NH_4^+	Hourly	Box 1: 24m Box 2: 41m	AGM / MBR
AMS	PM_1: NH_4^+, NO_3^-, SO_4^{2-}, Cl^-, Organics	5 Hz	32 m	EC
EcoPhysics CLD780TR	Canopy NO flux	5 Hz		EC
Automatic soil chamber	Soil flux of NO, NO_2, O_3			DCM
Ultrasonic anemometer	Sensible heat flux, u_*, L, U	Half hour	16 m, 24 m, 32 m, 41 m	EC
Thermocouple	Temperature	Half hour	16m, 24m, 32m, 41m	

EC: Eddy-covariance; AGM: aerodynamic gradient method; MBR: modified Bowen ratio method; DCM: dynamic chamber method

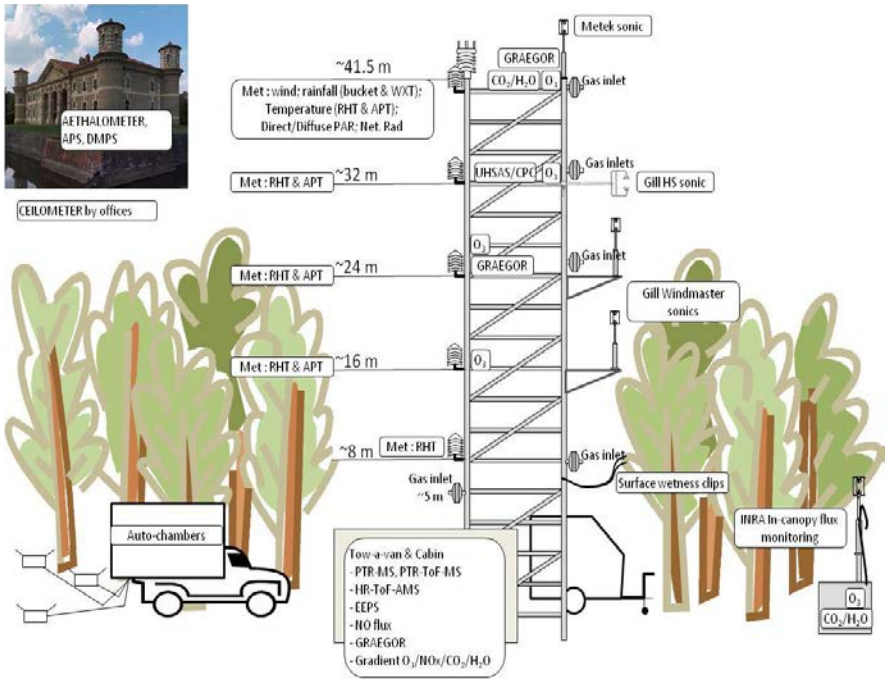

Figure 1. Layout of site at Bosco Fontana during the field campaign

2,2.1 GRAEGOR

The GRAEGOR system (GRadient of Aerosols and Gases Online Registration, ECN. Petten, Netherlands) (Thomas et al., 2009) is an online wet chemistry system, specifically designed for flux measurements using the aerodynamic gradient method (AGM), refer to Section 2.3 for further details. The GRAEGOR consists of 2 sampling boxes and 1 analyser box, which was housed in an air conditioned trailer during the campaign. The instrument uses an air pump sitting down stream of the 2 sampling boxes sampling at a flow rate of ~16.7 L / min . Air is first drawn through a 0.25 m PTFE inlet into a wet rotating annular denuder (WRD) containing a solution of 10 ppm H_2O_2. Gas molecules that are readily soluble diffuse into the liquid film in the denuder, whereas the remaining air stream enters a steam chamber contained within the steam jet aerosol collector (SJAC). Water soluble aerosols undergo rapid growth within in the chamber and are mechanically separated out of the air stream, which is collected at the bottom of the SJAC for analysis. Both the WRD and SJAC solutions are continually sampled at a constant flowrate of 0.33 ml/min by a set of alternating automated syringes contained in the analyser box at 30 minute cycles. In the analyser box, the 4 samples (WRD and SJAC each at two heights) are analysed in rotation by two different methods: 1) ion chromatography for Cl^-, NO_3^-, NO_2^- and SO_4^{2-}, 2) flow injection analysis (FIA) based on a selective ion membrane / conductivity cell for NH_4^+. A more detailed description of the GRAEGOR instrument and assessment of its applicability for fluxes can be found in Thomas et al. (2009) and Wolff et al. (2010).

Prior to analysis by chromatography the sample is first mixed with a NaBr internal standard (500 mg / L). The sample is then loaded onto a concentrator column (Dionex, IonPac, TAC-LP1, 4 × 35 mm) which is then injected onto an anion column (Dionex, IonPac, AG12,4 × 50 mm) using a 7 mM Na_2CO_3-8mM $NaHCO_3$ solution as the eluent. The sample is then analysed by chemical surpression, using a 50 mM solution of sulphuric acid. Concentrations of anions are calculated based on their specific conductivities compared to the internal standard, resulting in no need for a multi-point calibration to take place. Further details of the GRAEGOR instrument and its calibration can be found in Trebs et al. (2004) and Thomas et al. (2009). The FIA, on the other hand, requires frequent multipoint calibrations (every 72 hours during this campaign) with 0, 50, 500 ppb NH_4^+ solutions. As part of the QA/QC protocol the instrument was visually checked daily to ensure correct operation, as well as monitoring of waste flow, conductivity of deionised water and performance of the IC, as outlined by Thomas et al. (2009). In addition, the instrument air flow was checked and calibrated on a regular basis, with a independent flow meter to ensure no change in the flow rate and to enable correction of the air concentrations as part of the reanalysis procedure. During the first half of the campaign the two sample boxes were placed at 24 m on the tower, in order to resolve any issues due to pressure in sample lines, as the analyser box was at the ground level and solutions were transported through a micro bore tube between sample boxes. Once

performance of both sample boxes were in relative agreement, one of the sample boxes was moved to 42 m on the tower in order to do flux measurements.

2.2.2 HR-AMS

A high resolution time-of-flight Aerosol Mass Spectrometer (HR-AMS, Aerodyne Inc, US) was setup and operated inside the trailer adjacent to the foot of the tower (see Figure 1). The HR-AMS sub-sampled from the main inlet line (41 m) to provide chemically resolved concentrations measurements for the five main aerosol components – organics, nitrate, sulphate, ammonium and chloride. In addition to the standard concentration measurements, the instrument was also operated in an eddy covariance flux mode for 30 minutes within every hour. In concentration mode the AMS stepped between the V (high sensitivity mode), W (high m/z resolution mode) and particle time of flight modes (PToF) every five minutes. During the flux acquisition mode the air beam was blocked for the first and last minute of the 30 minute measurement period to provide an instrument background which was subsequently subtracted from the remaining 28 minutes.

2.2.3 NO_x measurements

Fluxes of NO were measured above the canopy, using a fast-response red-filtered chemiluminescence analyser (CLD780TR, EcoPhysics, Switzerland). Interference with other gases was accounted for by regular addition of excess O_3 to the pre-reaction chamber. The analyser achieves a detection limit of 90 ppt (3σ-definition).

In addition, the soil emission was NO was quantified using an automated chamber system with six chambers attached to a set of analysers, for NO, NO_2 and O_3 to account for the NO-NO_2-O_3 interactions.

2.3 Micrometeorology theory

In order to measure surface-atmosphere exchange near a surface it is assumed that the flux is constant with height and that surface within the footprint of the measured flux is homogenous. The ideal method to measure the flux (F_x) is through measuring instantaneous fluctuations of concentrations (χ') and the vertical wind component (w'):

$$F_x = \overline{w'\chi'} \qquad (1)$$

However, this method known as eddy covariance (EC) requires fast response instrumentation of several Hz. An alternative method is to derive fluxes by the aerodynamic gradient method (AGM), when fast response sensors are unavailable for the species of interest. The AGM derives the flux from a measurement of the vertical concentration gradient above the canopy (measurements at a minimum of two heights) and the flux-gradient relationship or eddy diffusivity (K_H) across the gradient.

$$F_x = K_H\left(\frac{z-d}{L}\right)\frac{d\chi}{dz} \qquad (2)$$

with

$$K_H\left(\frac{z-d}{L}\right) = \frac{(z-d)u_* k}{\phi_H\left(\frac{z-d}{L}\right)} \qquad (3)$$

Here u_* is the friction velocity, k is the von Karman constant (0.41), and ϕ_H is a correction for non-neutral stratification, provided by the universal functions, where stability is quantified by the Obukhov length (L). Eddy-diffusivity and universal functions scale with the height (z) relative to a zero plane displacement height (d), which, for a closed canopy, tends to be about 2/3 of the canopy height (h_c). In praxis the local gradient in Eq. (2) is approximated by the measurement of the gradient between two or more heights. To overcome the problem of having to calculate K_H for some arbitrary intermediate height, it can be shown that the flux can be calculated more pragmatically as (e.g. Flechard et al., 1997):

$$F_x = -ku_* \frac{\partial\chi}{\partial\left[\ln(z-d) - \Psi_H(\zeta)\right]} \qquad (4)$$

where Ψ_H is the integrated stability correction. The standard formulations of ϕ_H and Ψ_H can only be applied if measurements are taken above the surface roughness layer of the canopy, which typically extends to $2.3 \times h_c$, where profiles of concentrations and wind speed take on a logarithmic shape. This is a challenge for gradient measurements over forests because of the high canopy height and the need for a large homogeneous fetch when high measurements heights are used. Thus, corrections for the measurements within the surface roughness layer have been derived in several studies.

An alternative gradient method is the modified Bowen ratio (MBR) method in which similarity considerations are used to apply implicitly the flux-gradient relationship for an entrained entity (typically sensible heat), for which both the flux and gradient are known from independent sources, to another (the tracer of interest), without the need to calculate K_H or the universal functions explicitly. If the reference entity is heat, the flux can be calculated as (Huebert and Robert (1985)):

$$F_x = \frac{H}{\rho c_p}\frac{\Delta\chi}{\Delta T} \qquad (5)$$

where H is the sensible heat flux [W m^{-2}], ρ is the density of air and c_p is its heat capacity; T is temperature. An advantage of MBR is that it is independent of the universal functions and thus less empirical. The disadvantage is that it relies on similarity and also that it becomes uncertain when the reference flux is small. Thus, here MBR was only applied for $|H| > 40$ W m^{-2}.

From the calculated flux a (height dependent) deposition velocity ($V_d(z\text{-}d)$) of the pollutant can then be calculated as:

$$V_d(z-d) = -\frac{F}{\chi_a(z-d)} \quad (6)$$

The gradient approaches are only formulated for compounds that are chemically inert and need to be corrected when chemical sources / sinks exist between the different measurement heights. By contrast, for reactive compounds the eddy-covariance method derives a directly interpretable flux at the measurement height, which may, however, not reflect the true surface exchange, due to flux divergence.

2.4 Inferential modelling

Fluxes are often referred to being governed by a series of resistances, analogous to Ohms Law. HNO_3 and HCl fluxes are the simplest of the species measured to infer as it is proposed due to their sticky nature there is no surface resistance (R_c) to deposition. Instead it is assumed the total resistance (R_t) governing F_x is composed of two terms, the aerodynamic resistance (R_a) and the quasi laminar boundary layer resistance (R_b), where $R_t(z\text{-}d) = R_a(z\text{-}d) + R_b$:

$$F = \frac{-\chi_a(z_{ref})}{R_t(z-d)} \quad (7)$$

R_a is the resistance between the measurement height and the point near the surface where momentum is absorbed is referred to as the roughness height (z_0) calculated as:

$$R_a(z-d) = \frac{\ln\frac{(z-d)}{z_0} - \Psi_H(\zeta)}{ku_*} \quad (8)$$

At z_0, molecular diffusion becomes the controlling mechanism between the z_0 and the surface and is governed by R_b. There are various formulations for R_b which tend to give similar results over short vegetation, but diverge over aerodynamically rough surfaces such as forests.

We here explore two different formulations. Garland (1977) suggested the equation

$$R_b\{z-d\} = u*^{-1}\left[1.45\left(\frac{z_0 u*}{\nu}\right)^{0.24} Sc^{0.8}\right] \quad (9)$$

where Sc is the Schmidt number (ν/D) with D the molecular diffusivity of the property in air and ν the kinematic viscosity of air. Whilst an alternative equation results in larger R_b (Simpson et al., 2012):

$$R_b\{z-d\} = \frac{2}{ku*}\left(\frac{Sc}{\Pr}\right)^{2/3} \quad (10)$$

where *Pr* is the Prandtl number, a constant of 0.75.

The deposition of (an inert) tracer is always limited by R_a and R_b, but may be limited by further resistances reflecting the interaction with the vegetation. Thus, V_d cannot exceed the maximum deposition velocity

$$V_{max} = (R_a(z-d) + R_b)^{-1} \quad (11)$$

3 Results

3.1 Overview of meteorological conditions

This paper focuses on the period 27/06//12 and 10/07/12 when the GRAEGOR instrument was operated in gradient mode. Figure 2 presents a summary of the meteorology at the site for the period of interest. In addition to precipitation during instrument setup around 18 June, there were only 2 occasions with precipitation, both in close succession. A more detailed description of the meteorology and the associated data analysis can be found in Finco et al. (In preperation).

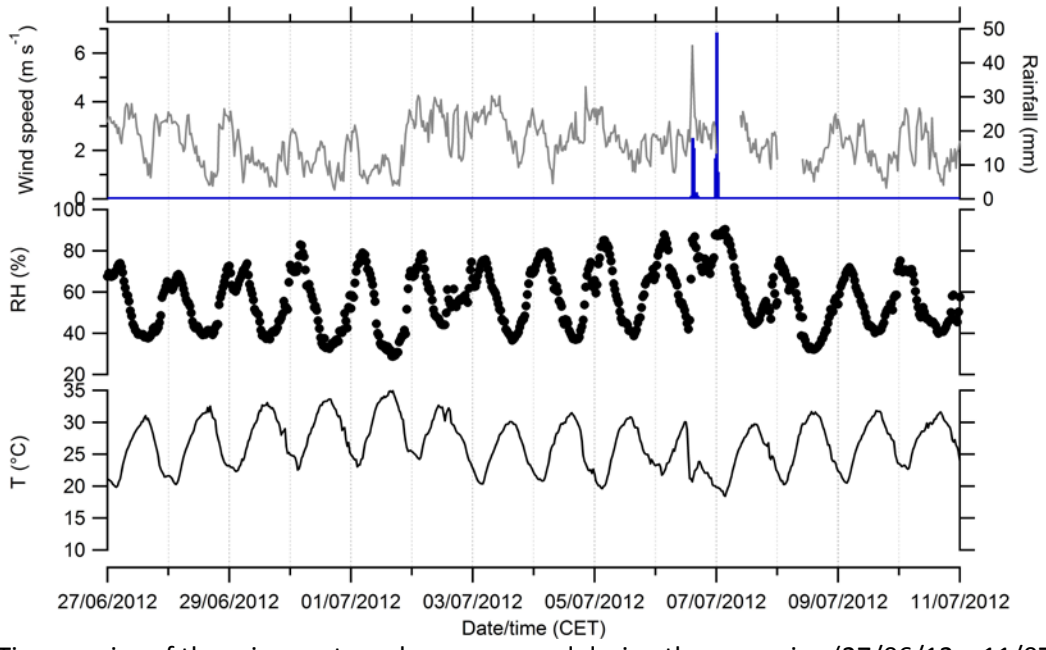

Figure 2. Times series of the micrometeorology measured during the campaign (27/06/12 – 11/07/12)

3.2 Concentrations

3.2.1 Gases

From the gas concentrations measured during the campaign (Figure 3), it is clear that concentrations of NH_3 and HNO_3 were elevated compared to other rural locations in Europe (Flechard et al., 2011). Ammonia concentrations ranged from 6.2 to 96.4 µg m^{-3} at 42 m during the period presented and appeared to be greatest when the wind was from a W-NW direction (Fig. 4). This is consistent with recent satellite data of the NH_3 column in the Po Valley which place the largest sources of NH_3 to the west of the site. Compared to other NH_3 measurements carried out concurrently in other locations in the Po Valley during the campaign (Sullivan et al., submitted), Bosco Fontana reported the highest NH_3 concentrations in the Po Valley region. Again this is believed to be due to geographic location, where the site is closer to emission sources and influenced by the topography of the region.

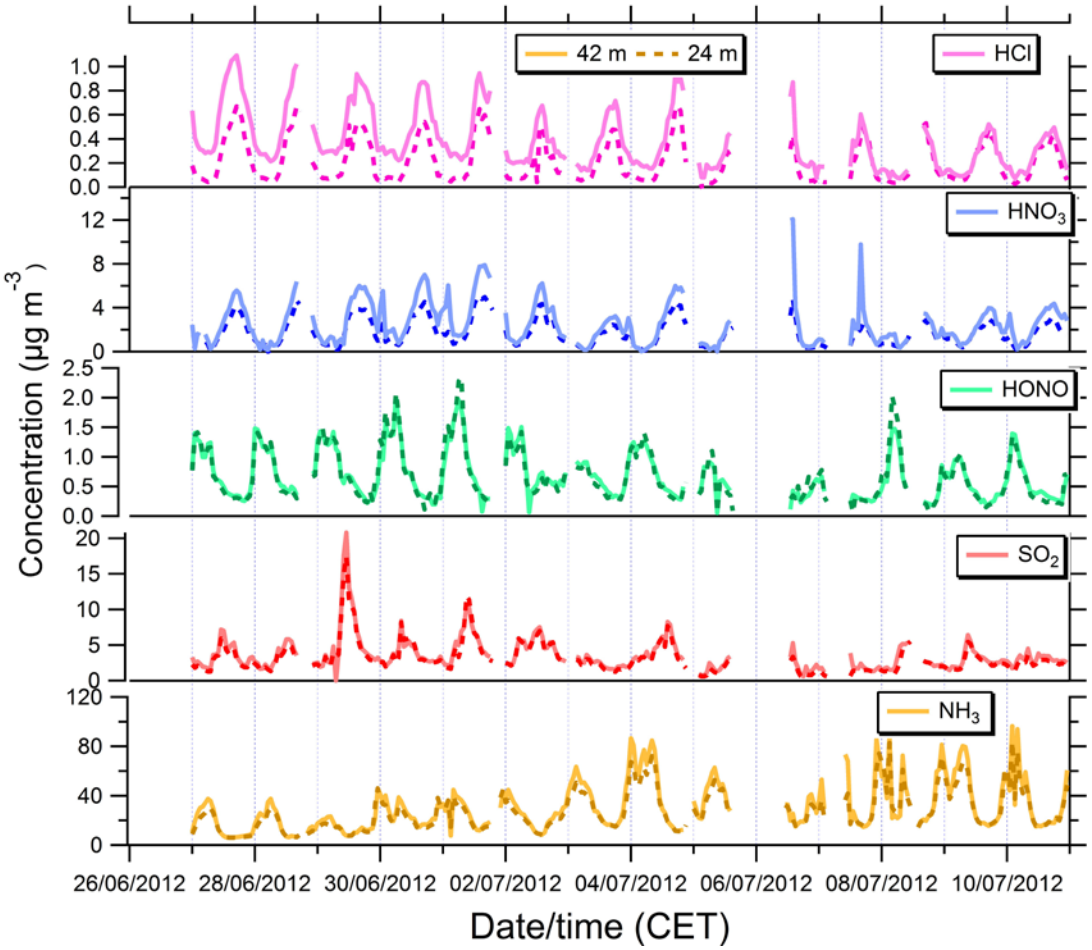

Figure 3. Time series (Central European Time, CET) of gas concentrations (NH_3, HNO_3 , HONO, HCl and SO_2) measured by the GRAEGOR at 24 m (dashed line) and 42 m (solid line) over Bosco Fontana at hourly resolution from 27/06 -11/07/2012

Nitric acid was also observed to be high, ranging from 0.02 to 12.08 µg m^{-3}, compared to other European rural locations (Auchencorth Moss, North UK (Twigg et al., 2015), Hyytiala, Finland (Makkonen et al., 2012)) and was of levels typically experienced in the urban environment across Europe. As previously

mentioned, HNO_3 will potentially have a N_2O_5 artefact, as described by Phillips et al. (2013), however it is going to be assumed under this scenario that all reported are HNO_3 as N_2O_5 would be transformed to HNO_3 at surface due to its interaction with H_2O on vegetation surfaces and therefore including N_2O_5 is not detrimental to assess the total N deposition to surfaces. Also, N_2O_5 is not stable during daytime and would only contribute to night-time measurements. Nitrous acid reported concentrations ranged from 0.05 to 1.99 µg m^{-3} at 41 m. It was generally observed that HONO concentrations decreased during the day and built up at night (Figure 3). This is not unexpected as HONO is generally thought to form in the troposphere at night due to the limited atmospheric lifetime during the day, as it undergoes rapid photolysis. It is unclear whether daytime values of HONO are exacerbated by a NO_x artefact which cannot be ruled out for such wet chemistry instruments.

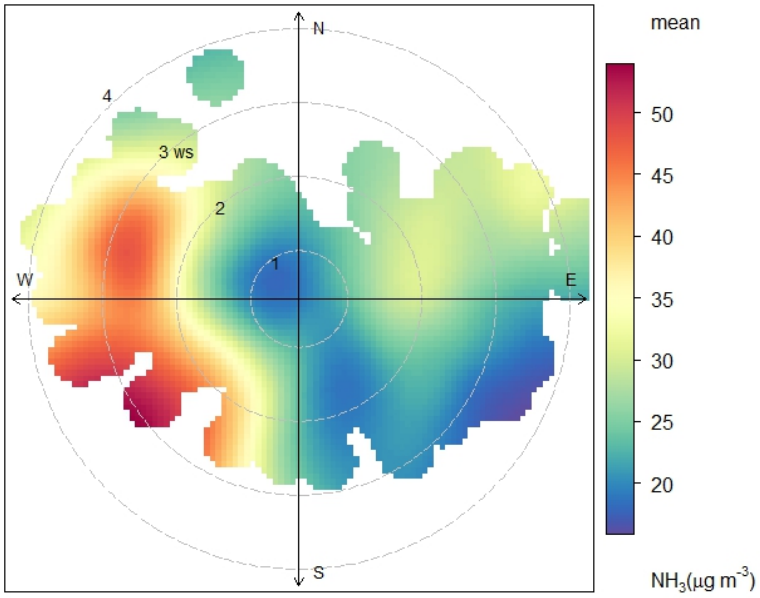

Figure 4. Polar plot of the mean NH_3 measured of by the GRAEGOR at Bosco Fontana at 41m with wind speed in m/s from the 27/06/12 to 10/07/12. (Graph produced using Open air; (Carslaw and Ropkins, 2012))

3.2.2 Aerosol chemical components

Figure 5 presents the time series for the period of the aerosol components measured by the GRAEGOR and the HR-AMS. It is clear that there are differences in the measurement of the two instruments, with the GRAEGOR consistently reporting higher NO_3^- concentrations than that reported by the AMS. One potential explanation is that the GRAEGOR measurement includes the reaction products of sea salt or crustal aerosol with HNO_3, which would not have been detected by the AMS for two reasons: firstly, these reaction products tend to be coarse (> 2.5 µm). The AMS only detects particles < 1 µm, whereas the GRAEGOR did not have a particulate cut-off and therefore would have measured any coarse NO_3^-, too. Secondly, the AMS only measures non-refractory particulate matter (aerosol that evaporates rapidly

at 600˚C), whereas these nitrates are refractory. In addition, the AMS had a 50 m long copper inlet and evaporation of volatile NH_4NO_3 inside this inlet cannot be ruled out, although the residence time was short (typically 6 s). By contrast, the AMS reported slightly larger concentrations for SO_4^{2-} than the GRAEGOR. NH_4^+ showed better agreement between the two instruments, though on the 04/07/12 the GRAEGOR observes a period of elevated concentrations, which was not seen by the AMS.

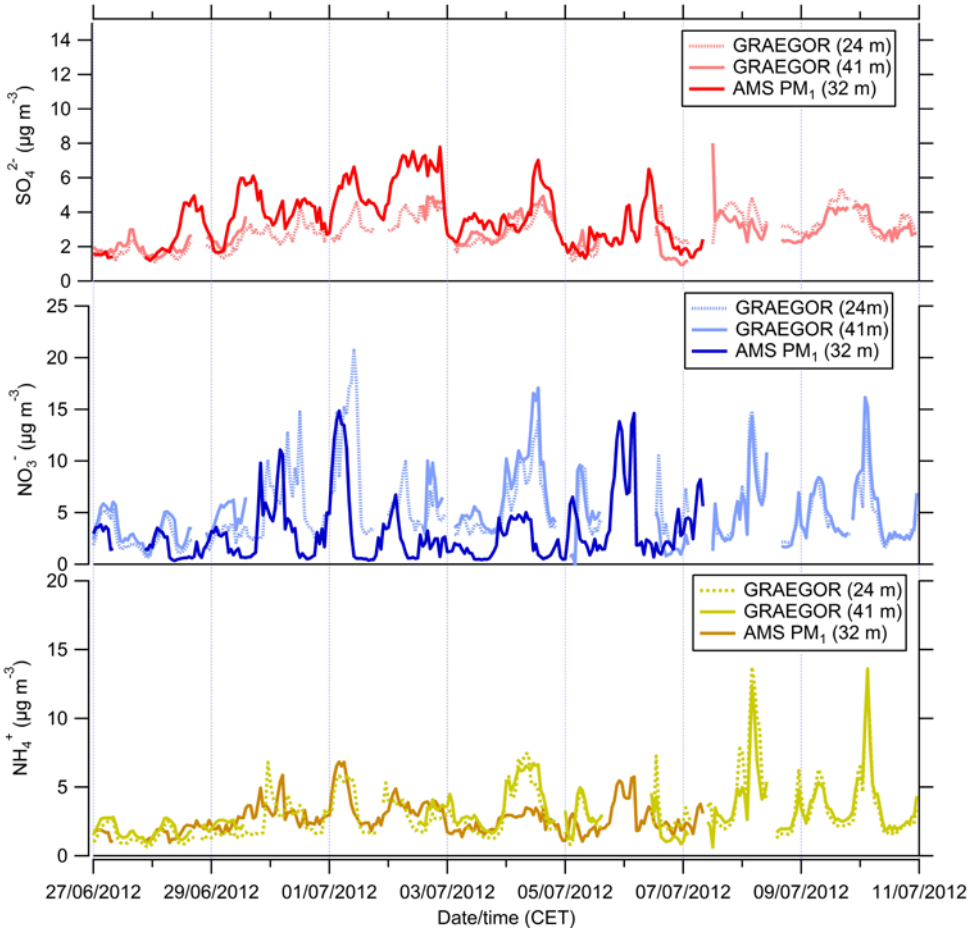

Figure 5. Time series of aerosol concentrations (NH_4^+, NO_3^-, Cl^- and SO_4^{2-}) measured by the GRAEGOR at 24 m and 41 m and AMS (32 m), which has a PM_1 cut-off over a hornbeam-oak forest at hourly resolution from 27/06 -11/07/2012.

3.3 Fluxes

3.3.1 Accounting for low measurement height

As mentioned in the methods section above, the application of AGM in forest roughness-layers is not straight-forward. Previous studies, also using the GRAEGOR, have demonstrated that there can be an underestimation in the flux (Wolff et al., 2010) over forests when measuring the roughness sublayer. During the Bosco Fontana campaign the lower measurement height of 24 m was low compared with the canopy height, with some canopy elements extending to 28 m, for logistic reasons out of our control. Thus, the required modification to the standard universal functions would be expected to be large and

there is the additional possibility that there may have been some exchange with the vegetation elements above the lower measurement height. Indeed, a comparison of the sensible heat fluxes which were measured at both heights (see Supplementary Information) indicate that the flux is not conserved and some heat is exchanged above the lower measurement height.

Some formulations of R_b have been derived from measured HNO_3 fluxes. Here we use the opposite approach to parameterise the effect of the low measurement height in the AGM approach. Instead of deriving a modified flux-profile relationship, we adjusted the displacement height until the AGM result matched the other flux estimates. Figure 6 compares the inferential model predictions of the HNO_3 flux based on the concentration measured at 41 m, using the two alternative formulations for Rb (Eqs. 9 and 10) and the result obtained with the MBR.

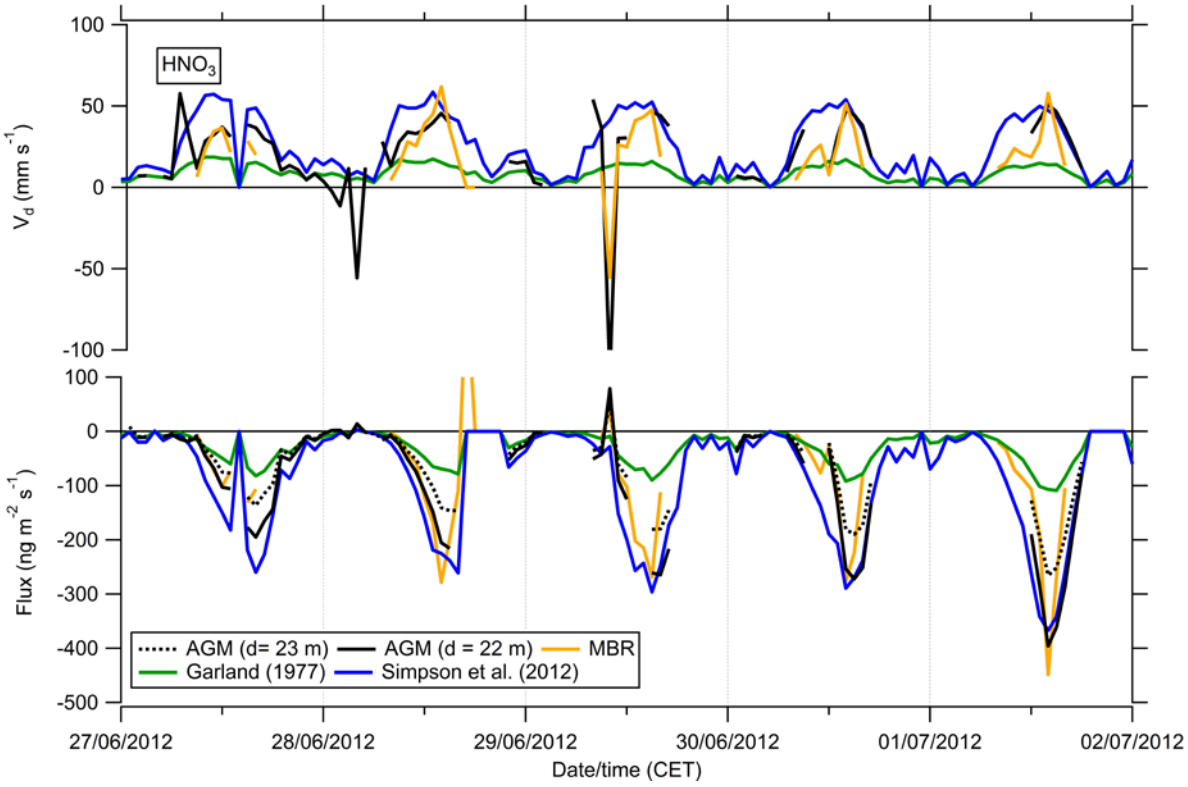

Figure 6. Comparison of unfiltered fluxes of HNO_3 calculated using the aerodynamic gradient method (AGM) with 1) d= 22 m and 2) d = 23 m, inferred fluxes assuming a zero R_c calculated with an R_b using 3) Garland (1977) or 4) Simpson et al. (2012) and 5) derived by the Modified Bowen Ratio (MBR) from the sensible heat flux measured at 41 m for 27/06/12 to 02/07/11. (Note: Fluxes were filtered where AGM was filtered when $u_* < 0.1$ m s^{-1} and $-1 < (z\text{-}d/L) > 1$, MBR was filtered when $H < 40$ W m^{-2} and $\Delta T < 0.5$ ˚C.)

Reasonable agreement was found between the MBR results and the inferential model using the R_b of Eq. (10), but the formulation of Garland (1977) (Eq. 9) tended to underestimate the deposition flux. The AGM results matches the MBR if a displacement height of 22 m is used, which is significantly larger than the one that would normally be applied for measurements outside the roughness layer ($d \approx 2/3 \times h_c \approx 18.7$ m).

Fluxes of reactive N compounds over Bosco Fontana

Based on the analysis in Section 3.3.1, fluxes were calculated using a displacement height of 22 m for the aerodynamic gradient method for the GRAEGOR instrument. A summary of the average and maximum fluxes, filtered for meteorological conditions during this period can be found in Table 2.

Table 2 Summary of concentrations (40.4 m) (EMEP method) measured at Bosco Fontana, Italy from the 27/06/12 to 10/07/12 by the GRAEGOR. Fluxes were calculated using AGM, with d = 22 m.

Species	Concentration (µg m^{-3})		Flux [a] (ng m^{-2} s^{-1})			V_d [b] (mm s^{-1})		DC
	Average	Max	Average	Min	Max	Average	Max	%
NH_3	30.43	96.40	-253.42	-1574.86	189.86	6.97	30.94	88
HNO_3	2.55	12.08	-65.37	-976.23	78.86	18.80	99.89	84
HONO	0.68	1.99	-3.60	-49.31	32.63	3.78	136.56	84
HCl	0.38	1.09	-14.72	-75.15	2.7	36.25	132.91	84
SO_2	3.55	20.80	-36.38	-564.15	157.95	9.72	145.33	84
NH_4^+	3.10	13.60	-44.11	-289.14	155.37	17.00	78.08	69
NO_3^-	4.97	17.09	-77.91	-594.75	346.91	11.80	79.99	64
Cl^-	0.41	2.08	-27.28	-351.12	1.2	50.76	168.55	64
SO_4^{2-}	2.80	8.01	-20.57	-1025.44	159.37	6.02	128.06	64

D.C = data capture of concentration data at 41 m; [a] fluxes are filtered for $-1 < (z-d)/L > 1$ and $u_* < 0.1$ m s^{-1}; [b] V_d was calculated using the measured concentration at 41 m and the calculated AGM flux (d = 22 m).

As expected for a semi-natural site situated in an extensively agricultural landscape, NH_3 was mainly deposited to the site and had the greatest deposition flux of all the N species measured by the GRAEGOR. During the day, there typically was a reduction in the deposition flux with some emission episodes during the time of 1400 to 2100 (CET) based on the median diurnal cycle for the period (Figure 7), which coincided with the lowest median concentrations observed at 41 m. The NH_3 flux was consistently smaller than V_{max} confirming the presence of a surface resistance and/or of non-zero emission potentials, either in the apoplast, on the leaf cuticle or soil/litter system.

The HNO_3 diurnal flux demonstrated that during the day deposition increased driven by an increase in concentration. This not surprising since HNO_3 primarily formed through photochemical reactions in the

atmosphere, resulting in greater concentrations above vegetation surface. When the measured flux by AMS for NO_3^- was compared to that from the GRAEGOR (Figure 7), it is apparent that the flux by the GRAEGOR is consistently larger. As previously discussed when studying the concentrations, there potentially was a loss of NO_3^- within the AMS inlet, which may explain the difference. However, the values of V_d measured by the two instruments at 41 m are in close agreement.

The HONO flux is much smaller than the other reactive N species measured by the GRAEGOR (Table 2). In the early morning there appears in the median diurnal cycle to be an early morning emission, one potential explanation is that this is due to evaporation of due at the leaf surface.

Annual dry deposition budget Bosco Fontana

Table 3 summarises the average fluxes of N compounds measured above Bosco Fontan and the annual N deposition they would equate for if they were representative of the entire year. NO_2 fluxes were not measured above the canopy and had to be estimated. An average NO flux of 39 ng NO-N m^{-2} s^{-1} was emitted by the soil, but the canopy-level NO flux was downwards except for some short episodes (Finco et al., in preparation). Because vegetation does not take up NO directly, the in-canopy sink for NO must have been reaction with O_3, which forms NO_2 a fraction of which would have been taken up by the canopy, whilst the remainder would have been emitted to the atmosphere.

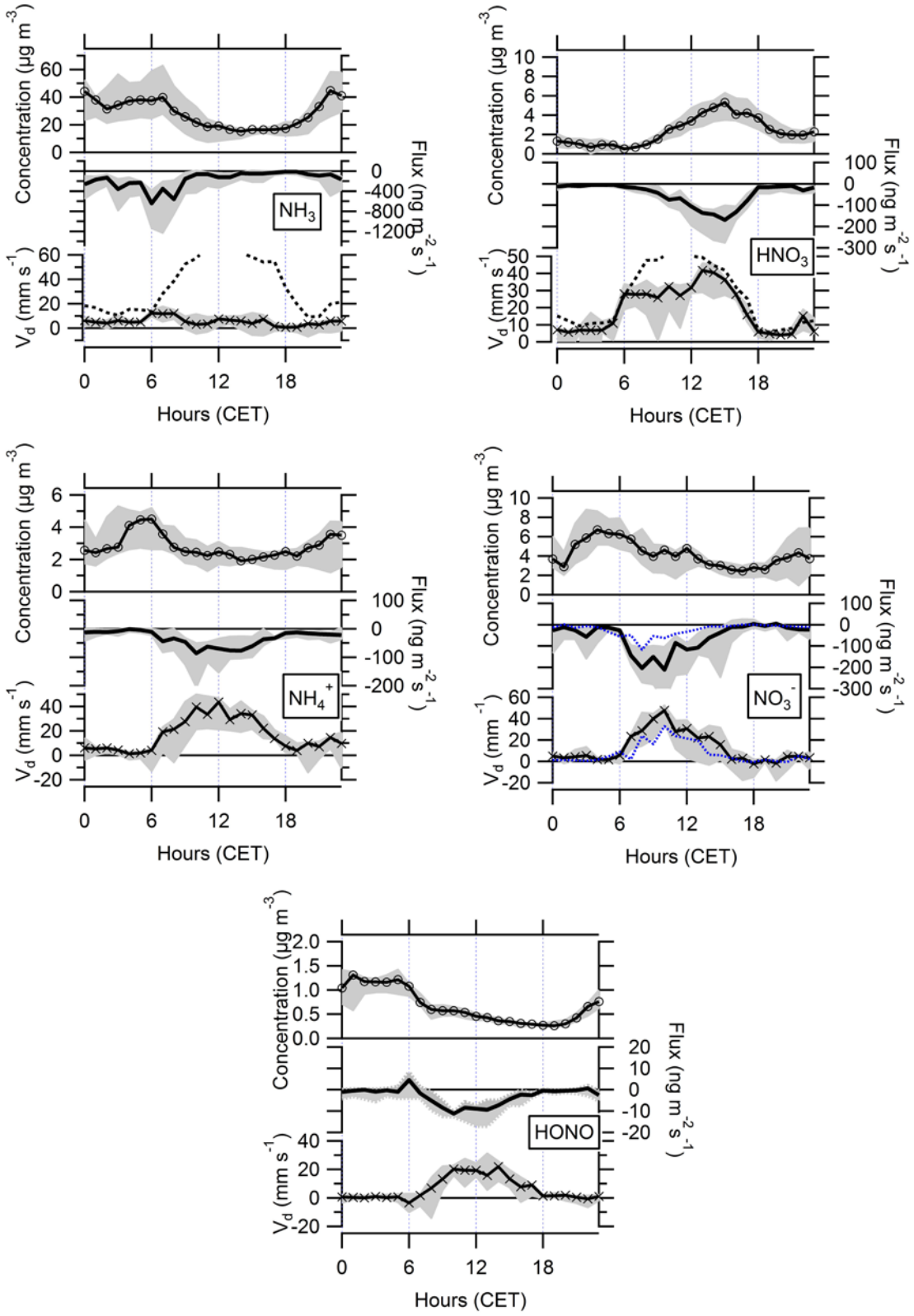

Fig 7. Median diurnal concentration (41 m) and fluxes (AGM method d = 22 m) of N species measured by the GRAEGOR at Bosco Fontana from the 27/06/12 – 10/07/12. Shaded area is the 25th to 75th percentiles of the measured flux. Filtered when u_* < 0.1 m s^{-1} and -1 m < (z-d) / L > 1 m. Blue lines in NO_3^- are F and V_d (calculated for 41 m, with a d = 22 m) measured by the HR-AMS. Dashed black line is the calculated V_{max}= $(R_a+R_b)^{-1}$.

Table 3 Annual N dry deposition budget at Bosco Fontana for the period 27/06/15 to 10/07/15 based on the average flux at the site for each species.

Species	Average flux during measurement period (ng N m^{-2} s^{-1})	Extrapolated annual deposition (kg N ha^{-1} yr^{-1})	Relative contribution to dry deposition of N (%)
NH_3 (1)	-208.7	65.8	74.7
HNO_3 (1)	-14.3	4.5	5.1
HONO (1)	-1.1	0.3	0.3
NO (2)	-3.5	1.1	1.3
NO_2 (3)	≈ 42.5	≈ - 4.0 (> -13.4)	Excluded
NH_4^+ (1)	-34.3	10.8	12.3
NO_3^- (1)	-17.6	5.5	6.3
Total	**-237**	**-74.7**	**100**
NO (soil) (4)	39.0	12.3	Excluded

Instrument and flux method: (1)GRAEGOR and AGM, (2)EcoPhyics and EC; (3)Estimated as 0.3 times the total NO entering the canopy air space; (4) dynamic soil chamber

To estimate a budget with the atmosphere, we have assumed that on average 30% of the NO_2 produced escapes the canopy. This results in a net flux with the atmosphere of -74.7 kg N ha^{-1} yr^{-1} from dry deposition alone. This does not include the amount of soil NO that is re-absorbed as NO_2 as this constitutes internal cycling.

4 Discussion

4.1 Deviation of fluxes over forests

4.1.1 State of gas-particle partitioning

To assess whether the gas-particle partitioning is in thermodynamic equilibrium, a partitioning model (ISORROPIA II, (Fountoukis and Nenes, 2007)) was applied to the dataset. The model was operated in the forward reaction and with the aerosols in thermodynamically stable state, where salts precipitate if saturation is exceeded. An initial run was carried out using the input of the measured total ammonium (TA= NH_3 + NH_4^+), total nitrate (TN = HNO_3 + NO_3^-) and SO_4^{2-} only in µmol m^{-3}. To check that the Cl^- was not greatly modifying the thermodynamics, the run was repeated including total Cl^- and, in the

absence of Na^+ measurements, a calculated Na^+ value. The Na^+ was calculated using data from a study which was run in parallel further south in the Po Valley at San Pietro Capofiume (SPC), 92 km SE of Bosco Fontana. The method to obtain the data at SPC is a similar online IC method but using cation IC instead of FIA, called the MARGA (Metrohm-Applikon, NL). Further details of the MARGA instrument can be found in the Supplementary Material. The MARGA at SPC used a PM_{10} cut-off (10 µm aerodynamic diameter). The measured PM_{10} Cl^- at SPC was then compared to the GRAEGOR Cl^- at Bosco Fontana. The data was found to have a similiar magnitude and temporal pattern (Supplementary Material). As a result, the linear regression of Na:Cl ratio at SPC was applied to calculate Na^+ for Bosco Fontana using the measured Cl^- at Bosco Fontana. From Figure 8, it is apparent that the introduction of Na^+ and Cl^- does not appear on inspection of the time series to alter the gas aerosol partitioning of the NH_3-HNO_3-NH_4NO_3 system. The fact that this second run overestimates the amount of free HCl may suggests that a larger fraction of the aerosol Cl^- is tied to Na^+ rather than available to form volatile NH_4Cl than would be predicted by the SPC ratio. As a result the effect of HCl on the NH_3 partitioning might be even smaller in reality.

The ISORROPIA model appears to fit the NH_3 time series well, which is not surprising given that TA is completely dominated by the gas phase in both the model and the measurements. However, NH_4^+ is consistently underestimated and the NO_3^- is also underestimated, though there are periods of reasonable agreement. The model suggests that there should be no NO_3^- during the day and instead be partitioned to the gas phase HNO_3. For HNO_3 the temporal variations between measured and modelled are comparable, however, the model consistently overestimates the HNO_3 at the site, which is most likely due to not predicting the presence of NO_3^- during the day.

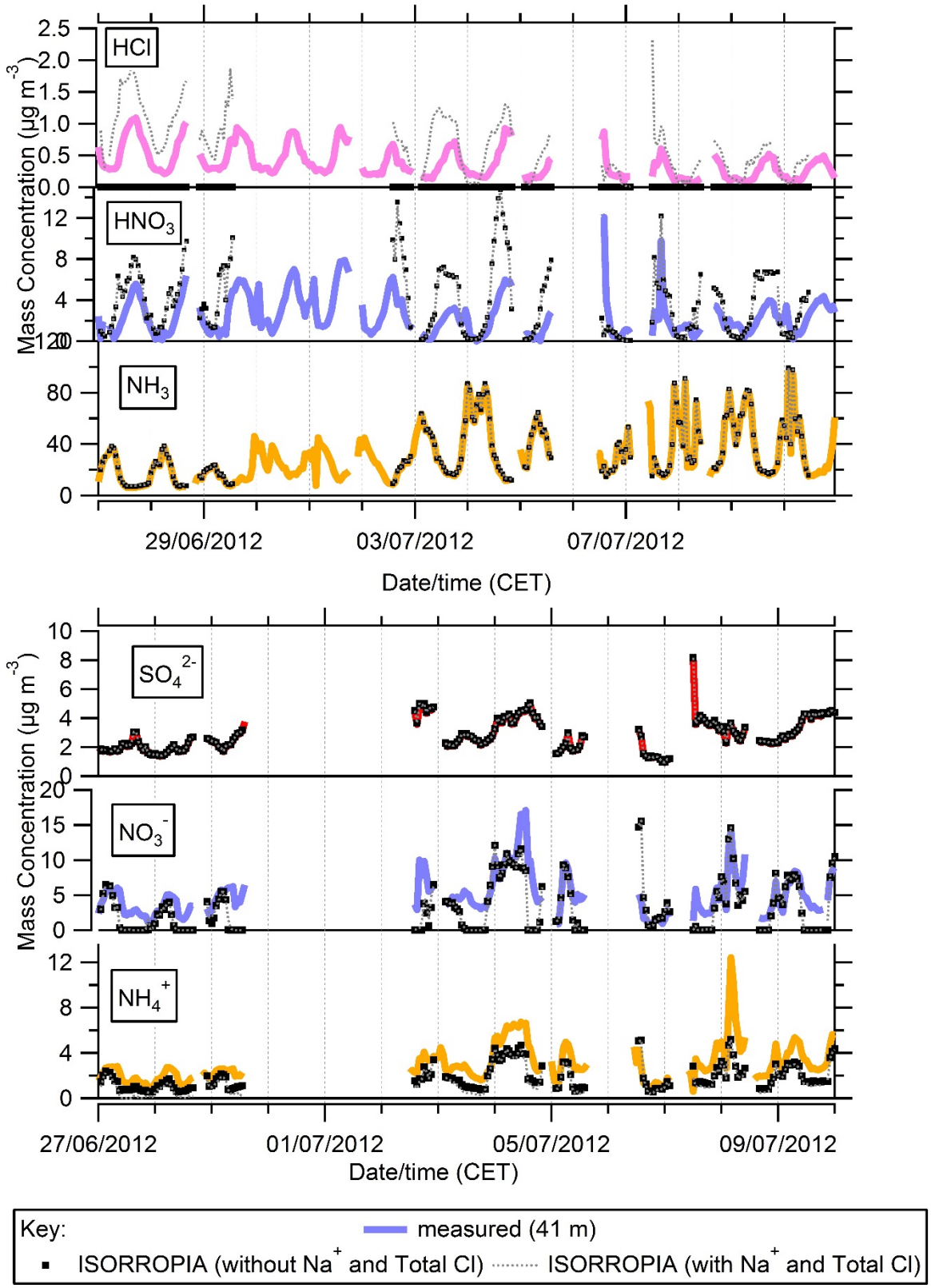

Figure 8 Measured concentrations at 41 m (solid line) compared to the ISORROPIA model II (dashed line)

As mentioned above, the observation of daytime NO_3^- cannot be fully attributed to non-volatile forms of NO_3^- (i.e. $NaNO_3$) as this observation was also made with the AMS which is insensitive to these refractory forms. Instead, the model/measurement comparison strongly suggests that the gas-aerosol partitioning is perturbed due to interactions between partitioning and vertical transport. During the day, as individual particles approach the forest canopy, they enter a region of warmer temperatures where gas-phase concentrations are depleted due to the effect of deposition gradients. Whilst NH_4NO_3 may be predicted to exist at higher heights (where temperatures are colder and gas concentrations higher), even at the conditions at the measurement height NH_4NO_3 should have fully evaporated. However, kinetic constraints does not allow equilibrium to be re-attained sufficiently rapidly during the deposition process. Given that the conditions favour evaporation at the measurement height, the drivers for evaporation are even stronger below the measurement height where temperature further increases and gas-phase concentrations are even smaller.

4.1.2 Effects of aerosol evaporation on surface exchange fluxes

Particles in the accumulation mode, where NH_4^+ and NO_3^- are found tend to deposit at rates of 1 to 20 mm s^{-1} to forest and this was supported by the AMS flux measurements of SO_4^{2-} which showed a noisy time series with values < 10 mm s^{-1} (not shown). Instead, NO_3^- and NH_4^+ both show much higher V_d that peak during the day at 40 mm s^{-1} on average, suggesting that additional sinks for these compounds exist below the measurement height that are not regulated by physical interactions of the particles with the canopy. In previous studies (Nemitz et al., 2004; Nemitz and Sutton, 2004; Ryder, 2010) we have demonstrated that these high apparent deposition rates are consistent with NH_4NO_3 evaporation during the deposition process. Thus, some of the NH_4^+ and NO_3^- do not deposit in particulate phase, but are driven off the aerosol and are then either deposited (more effectively) in gaseous form or re-released to the atmosphere.

HNO_3 is expected to deposit at V_{max} with a zero canopy resistance. Thus, negative deviations from V_{max} can be taken as an indication that there is a non-zero vapour pressure or source of HNO_3 below the measurement height (e.g. Nemitz et al., 2004). At Bosco Fontana the deposition of HNO_3 suggested reduced deposition between 6:00 and 13:00, exactly during the same time when NO_3^- deposition fluxes were largest. Although the apparent deposition rate of both HNO_3 and NO_3^- aerosol reached on average 35 to 40 mm s^{-1}, it fell short of the average V_{max} of 50 mm s^{-1}. This indicates that the evaporation of NH_4NO_3 was reasonably fast (to bring $V_d(NO_3^-)$ to similar values as $V_d(HNO_3)$ but not instantaneous, in which case V_d(TN) would have equalled V_{max}. This implies that the majority (but not all) of the HNO_3 that is driven off the aerosol deposits efficiently rather than being re-released to the atmosphere.

Because the gas-aerosol partitioning clearly changed between the two measurement heights used for the AGM, a basic condition for the applicability of AGM is violated. It is well recognised that in this process the fluxes of TN and TA remain conserved with height (e.g. Wolff et al., 2011). Whilst we do not present fluxes of TN and TA explicitly, the way the individual fluxes were calculated implies that F_{TN} can be calculated accurately as $F_{TN} = F_{NH3} + F_{NH4+}$ even if the component fluxes are subject to an error. The same applies to F_{TA}. Thus, the N budgets remain robust.

4.2 N deposition budget for Bosco Fontana

As expected the N flux was large. Based on measurements an annual total deposition of almost 75 kg N ha^{-1} yr^{-1} was calculated for Bosco Fontana. This estimate is based on the approximation that this summer period is representative for the year, which is almost certainly not the case. With fluxes dominated by NH_3, winter NH_3 concentrations may be smaller (e.g. due to the temperature response of emissions, the reduced fertiliser use in winter and the gas-aerosol partitioning being shifted towards the aerosol phase), but their deposition to wet winter canopies may be more efficient, despite the absence of leaves. The expected higher winter concentrations of aerosol NH_4^+ and NO_3^- would not undergo the same fast effective deposition observed during summer, because the vegetation canopies are not as warm relative to air temperatures.

Bulk deposition was measured to be in the region of 40 kg N ha^{-1} yr^{-1} in the S. Po Valley.

The annual total calculated here is much larger than that measured by throughfall measurements at the site, where Ferretti et al. (2014) in the same region calculate a N deposition of ~ 28.8 kg N ha^{-1} yr^{-1} based on the sum of N-NH_4 and N-NO_3. There are a number of reasons why the magnitude of the dry deposition flux of N varies, in addition to the poor coverage of our measurements: the trees within the forest are most likely to take up N and therefore reduce N at the surface and the throughfall method could also have suffered losses through volatilisation and offline analysis.

5 Conclusions

The N dry deposition to Bosco Fontana, an extreme case of aerodynamically rough, semi-natural vegetation situated at the heart of one of the most N polluted areas Europe's, was large, averaging 209 ng N m^{-2} s^{-1}, which equates to an annual input of 74.7 kg N ha^{-1} yr^{-1}, well above the N Critical Load for (meso- and eutrophic) *Quercus* woodlands of 15 to 20 kg N ha^{-1} yr^{-1}, even without taking into account any additional wet deposition. This flux is dominated by ammonia (75%), but fine aerosol (NH_4^+ and NO_3^-) make a substantial (jointly 18%) contribution and HNO_3 adds a further 5%. Atmospheric deposition of NO and HONO are of minor importance. A long-term dataset would be required to assess

the robustness of the annual budgets. The high N inputs explain the unusually large soil NO emissions observed at this site (Finco et al., in preparation).

The collocation of instrumentation from several groups within the context of the ECLAIRE Integrated Experiment provided a useful dataset to assess the importance of the interaction between surface / atmosphere exchange and gas-particle re-partitioning. The thermodynamic model suggest that NH_4NO_3 should not exist at the conditions found at the measurement height. But particles transported down from a higher height, where daytime temperatures are cooler and gas concentrations less depleted due to the deposition process, contain remnants of volatile compounds. These continue to evaporate at and below the measurement height, resulting in the observation of large effective deposition rates of NH_4^+ and NO_3^- as well as slightly reduced deposition rates of HNO_3 during midday. Interestingly, the deposition rate of total nitrate (TN = NO_3^- + HNO_3) reaches about 75% of the deposition rate expected for pure HNO_3, suggesting that evaporation is fast but not instantaneous. This suggest that much but not all of the HNO3 released is deposited locally. A modelling exercise should follow to better constrain the observations and to derive subgrid parameterisations as well as empirical parameterisations to account for the enhancement in aerosol deposition in chemistry and transport models.

6 Acknowledgements

We gratefully acknowledge support from the project "Effects of Climate Change on Air Pollution Impacts and Response Strategies for European Ecosystems" (ÉCLAIRE), funded under the EC 7th Framework Programme (Grant Agreement No. 282910).

References

Acton, W. J. F., Schallhart, S., Langford, B., Valach, A., Rantala, P., Fares, S., Carriero, G., Tillmann, R., Tomlinson, S. J., Dragosits, U., Gianelle, D., Hewitt, C. N., and Nemitz, E.: Canopy-scale flux measurements and bottom-up emission estimates of volatile organic compounds from a mixed oak and hornbeam forest in northern Italy, Atmos. Chem. Phys. Discuss., 15, 29213-29264, 10.5194/acpd-15-29213-2015, 2015.

Bigi, A., Ghermandi, G., and Harrison, R. M.: Analysis of the air pollution climate at a background site in the Po valley, Journal of Environmental Monitoring, 14, 552-563, 10.1039/c1em10728c, 2012.

Carslaw, D. C., and Ropkins, K.: Openair — an R package for air quality data analysis. , Environmental Modelling & Software. , 27-28, 52–61, 2012.

Dalponte, M., Bruzzone, L., and Gianelle, D.: Fusion of hyperspectral and LIDAR remote sensing data for classification of complex forest areas, , IEEE T. Geosci. Remote, 46, 1416–1427, 2008.

Decesari, S., Facchini, M. C., Matta, E., Lettini, F., Mircea, M., Fuzzi, S., Tagliavini, E., and Putaud, J. P.: Chemical features and seasonal variation of fine aerosol water-soluble organic

compounds in the Po Valley, Italy, Atmospheric Environment, 35, 3691-3699, http://dx.doi.org/10.1016/S1352-2310(00)00509-4, 2001.

Decesari, S., Allan, J., Plass-Duelmer, C., Williams, B. J., Paglione, M., Facchini, M. C., O'Dowd, C., Harrison, R. M., Gietl, J. K., Coe, H., Giulianelli, L., Gobbi, G. P., Lanconelli, C., Carbone, C., Worsnop, D., Lambe, A. T., Ahern, A. T., Moretti, F., Tagliavini, E., Elste, T., Gilge, S., Zhang, Y., and Dall'Osto, M.: Measurements of the aerosol chemical composition and mixing state in the Po Valley using multiple spectroscopic techniques, Atmos. Chem. Phys., 14, 12109-12132, 10.5194/acp-14-12109-2014, 2014.

Ferrara, R. M., Loubet, B., Di Tommasi, P., Bertolini, T., Magliulo, V., Cellier, P., Eugster, W., and Rana, G.: Eddy covariance measurement of ammonia fluxes: Comparison of high frequency correction methodologies, Agricultural and Forest Meteorology, 158–159, 30-42, http://dx.doi.org/10.1016/j.agrformet.2012.02.001, 2012.

Ferretti, M., Marchetto, A., Arisci, S., Bussotti, F., Calderisi, M., Carnicelli, S., Cecchini, G., Fabbio, G., Bertini, G., Matteucci, G., de Cinti, B., Salvati, L., and Pompei, E.: On the tracks of Nitrogen deposition effects on temperate forests at their southern European range – an observational study from Italy, Global Change Biology, 20, 3423-3438, 10.1111/gcb.12552, 2014.

Finco, A., Coyle, M., Marzuoli, R., Nemitz, E., and Gerosa, G.: TBD In preperation.

Flechard, C. R., Nemitz, E., Smith, R. I., Fowler, D., Vermeulen, A. T., Bleeker, A., Erisman, J. W., Simpson, D., Zhang, L., Tang, Y. S., and Sutton, M. A.: Dry deposition of reactive nitrogen to European ecosystems: a comparison of inferential models across the NitroEurope network, Atmos. Chem. Phys., 11, 2703-2728, 10.5194/acp-11-2703-2011, 2011.

Fountoukis, C., and Nenes, A.: ISORROPIA II: a computationally efficient thermodynamic equilibrium model for K+–Ca2+–Mg2+–NH4+–Na+–SO42−–NO3−–Cl−–H2O aerosols, Atmos. Chem. Phys., 7, 4639-4659, 10.5194/acp-7-4639-2007, 2007.

Fowler, D., Steadman, C. E., Stevenson, D., Coyle, M., Rees, R. M., Skiba, U. M., Sutton, M. A., Cape, J. N., Dore, A. J., Vieno, M., Simpson, D., Zaehle, S., Stocker, B. D., Rinaldi, M., Facchini, M. C., Flechard, C. R., Nemitz, E., Twigg, M., Erisman, J. W., and Galloway, J. N.: Effects of global change during the 21st century on the nitrogen cycle, Atmos. Chem. Phys. Discuss., 15, 1747-1868, 10.5194/acpd-15-1747-2015, 2015.

Garland, J. A.: The Dry Deposition of Sulphur Dioxide to Land and Water Surfaces, Proceedings of the Royal Society of London A: Mathematical, Physical and Engineering Sciences, 354, 245-268, 10.1098/rspa.1977.0066, 1977.

Kleffmann, J., Gavriloaiei, T., Hofzumahaus, A., Holland, F., Koppmann, R., Rupp, L., Schlosser, E., Siese, M., and Wahner, A.: Daytime formation of nitrous acid: A major source of OH radicals in a forest, Geophysical Research Letters, 32, n/a-n/a, 10.1029/2005gl022524, 2005.

Makkonen, U., Virkkula, A., Mäntykenttä, J., Hakola, H., Keronen, P., Vakkari, V., and Aalto, P. P.: Semi-continuous gas and inorganic aerosol measurements at a Finnish urban site: comparisons with filters, nitrogen in aerosol and gas phases, and aerosol acidity, Atmos. Chem. Phys., 12, 5617-5631, 10.5194/acp-12-5617-2012, 2012.

Matta, E., Facchini, M. C., Decesari, S., Mircea, M., Cavalli, F., Fuzzi, S., Putaud, J. P., and Dell'Acqua, A.: Mass closure on the chemical species in size-segregated atmospheric aerosol collected in an urban area of the Po Valley, Italy, Atmos. Chem. Phys., 3, 623-637, 10.5194/acp-3-623-2003, 2003.

Mélin, F., and Zibordi, G.: Aerosol variability in the Po Valley analyzed from automated optical measurements, Geophysical Research Letters, 32, n/a-n/a, 10.1029/2004gl021787, 2005.

Phillips, G. J., Makkonen, U., Schuster, G., Sobanski, N., Hakola, H., and Crowley, J. N.: The detection of nocturnal N2O5 as HNO3 by alkali- and aqueous-denuder techniques, Atmos. Meas. Tech., 6, 231-237, 10.5194/amt-6-231-2013, 2013.

Pogány, A., Mohácsi, Á., Jones, S. K., Nemitz, E., Varga, A., Bozóki, Z., Galbács, Z., Weidinger, T., Horváth, L., and Szabó, G.: Evaluation of a diode laser based photoacoustic instrument combined with preconcentration sampling for measuring surface–atmosphere exchange of ammonia with the aerodynamic gradient method, Atmospheric Environment, 44, 1490-1496, **http://dx.doi.org/10.1016/j.atmosenv.2010.01.038**, 2010.

Roscioli, J. R., Zahniser, M. S., Nelson, D. D., Herndon, S. C., and Kolb, C. E.: New Approaches to Measuring Sticky Molecules: Improvement of Instrumental Response Times Using Active Passivation, The Journal of Physical Chemistry A, 10.1021/acs.jpca.5b04395, 2015.

Rumsey, I. C., Cowen, K. A., Walker, J. T., Kelly, T. J., Hanft, E. A., Mishoe, K., Rogers, C., Proost, R., Beachley, G. M., Lear, G., Frelink, T., and Otjes, R. P.: An assessment of the performance of the Monitor for AeRosols and GAses in ambient air (MARGA): a semi-continuous method for soluble compounds, Atmos. Chem. Phys., 14, 5639-5658, 10.5194/acp-14-5639-2014, 2014.

Simpson, D., Benedictow, A., Berge, H., Bergström, R., Emberson, L. D., Fagerli, H., Flechard, C. R., Hayman, G. D., Gauss, M., Jonson, J. E., Jenkin, M. E., Nyíri, A., Richter, C., Semeena, V. S., Tsyro, S., Tuovinen, J. P., Valdebenito, Á., and Wind, P.: The EMEP MSC-W chemical transport model – technical description, Atmos. Chem. Phys., 12, 7825-7865, 10.5194/acp-12-7825-2012, 2012.

Sintermann, J., Spirig, C., Jordan, A., Kuhn, U., Ammann, C., and Neftel, A.: Eddy covariance flux measurements of ammonia by high temperature chemical ionisation mass spectrometry, Atmos. Meas. Tech., 4, 599-616, 10.5194/amt-4-599-2011, 2011.

Sörgel, M., Trebs, I., Wu, D., and Held, A.: A comparison of measured HONO uptake and release with calculated source strengths in a heterogeneous forest environment, Atmos. Chem. Phys., 15, 9237-9251, 10.5194/acp-15-9237-2015, 2015.

Sullivan, A. P., Hodas, N., Turpin, B. J., Skog, K., Keutsch, F. N., Gilardoni, S., Paglione, M., Rinaldi, M., Decesari, S., Facchini, M. C., Poulain, L., Herrmann, H., Wiedensohler, A., Nemitz, E., Twigg, M. M., and Collett, J. L.: Evidence for Ambient Dark Aqueous SOA Formation in the Po Valley, Italy, submitted.

Sutton, M. A., Reis, S., and Baker, S. M. H.: Atmospheric Ammonia - Detecting emission changes and environmental impacts. Results of an Expert Workshop under the Convention on Long-range Transboundary Air Pollution., Springer, 2009.

Thomas, R. M., Trebs, I., Otjes, R., Jongejan, P. A. C., Brink, H. t., Phillips, G., Kortner, M., Meixner, F. X., and Nemitz, E.: An Automated Analyzer to Measure Surface-Atmosphere Exchange Fluxes of Water Soluble Inorganic Aerosol Compounds and Reactive Trace Gases, Environmental Science & Technology, 43, 1412-1418, 10.1021/es8019403, 2009.

Trebs, I., Meixner, F. X., Slanina, J., Otjes, R., Jongejan, P., and Andreae, M. O.: Real-time measurements of ammonia, acidic trace gases and water-soluble inorganic aerosol species at a rural site in the Amazon Basin, Atmos. Chem. Phys., 4, 967-987, 10.5194/acp-4-967-2004, 2004.

Twigg, M. M., House, E., Thomas, R., Whitehead, J., Phillips, G. J., Famulari, D., Fowler, D., Gallagher, M. W., Cape, J. N., Sutton, M. A., and Nemitz, E.: Surface/atmosphere exchange

and chemical interactions of reactive nitrogen compounds above a manured grassland, Agricultural and Forest Meteorology, 151, 1488-1503, http://dx.doi.org/10.1016/j.agrformet.2011.06.005, 2011.

Twigg, M. M., Di Marco, C. F., Leeson, S., van Dijk, N., Jones, M. R., Leith, I. D., Morrison, E., Coyle, M., Proost, R., Peeters, A. N. M., Lemon, E., Frelink, T., Braban, C. F., Nemitz, E., and Cape, J. N.: Water soluble aerosols and gases at a UK background site – Part 1: Controls of PM2.5 and PM10 aerosol composition, Atmos. Chem. Phys., 15, 8131-8145, 10.5194/acp-15-8131-2015, 2015.

Van Damme, M., Wichink Kruit, R. J., Schaap, M., Clarisse, L., Clerbaux, C., Coheur, P. F., Dammers, E., Dolman, A. J., and Erisman, J. W.: Evaluating 4 years of atmospheric ammonia (NH_3) over Europe using IASI satellite observations and LOTOS-EUROS model results, Journal of Geophysical Research: Atmospheres, 119, 9549-9566, 10.1002/2014jd021911, 2014.

Volpe Horii, C., William Munger, J., Wofsy, S. C., Zahniser, M., Nelson, D., and Barry McManus, J.: Atmospheric reactive nitrogen concentration and flux budgets at a Northeastern U.S. forest site, Agricultural and Forest Meteorology, 133, 210-225, http://dx.doi.org/10.1016/j.agrformet.2004.08.009, 2005.

Whitehead, J. D., Twigg, M., Famulari, D., Nemitz, E., Sutton, M. A., Gallagher, M. W., and Fowler, D.: Evaluation of Laser Absorption Spectroscopic Techniques for Eddy Covariance Flux Measurements of Ammonia, Environmental Science & Technology, 42, 2041-2046, 10.1021/es071596u, 2008.

Wolff, V., Trebs, I., Ammann, C., and Meixner, F. X.: Aerodynamic gradient measurements of the NH_3-HNO_3-NH_4NO_3 triad using a wet chemical instrument: an analysis of precision requirements and flux errors, Atmos. Meas. Tech., 3, 187-208, 10.5194/amt-3-187-2010, 2010.

Zhu, T., Melamed, M., Parrish, D., Gauss, M., Gallardo, K. L., Lawrence, M., Konare, A., and Liousse, C.: WMO/IGAC Impacts of Megacities on Air Pollution and Climate., Geneva, Switzerland,, 2012.

Supplementary Information

Controls of reactive nitrogen fluxes and gas-aerosol interactions above a semi-natural forest in the Po Valley, Italy.

Twigg, M.M.[1] Di Marco, C.F. [1] Langford, B. [1] Loubet, B.[2] Gerosa, G.[3] Finco, A.[3] Sutton, M.A.[1] Nemitz, E.[1]

To understand if the measurement heights used by the GRAEGOR instrument were within the canopy, a comparison of the sensible heat (*H*) which was measured by eddy covariance at a number of heights during the campaign was compared (Figure S1). It is clear that at 24 m the flux has been dampened and therefore must be already within the canopy. The sensible heat flux was calculated using thermocouple measurements at the same height as the GRAEGOR (24 m and 41 m) by traditional aerodynamic gradient method (AGM) refer to section 2.3 in the main manuscript for details of this method, where it is assumed that $d=2/3h_c$, where h_c is the canopy height. It was found that the flux by AGM was also dampened resulting in a flux of similar magnitude to that of the *H* measured by EC at 24 m.

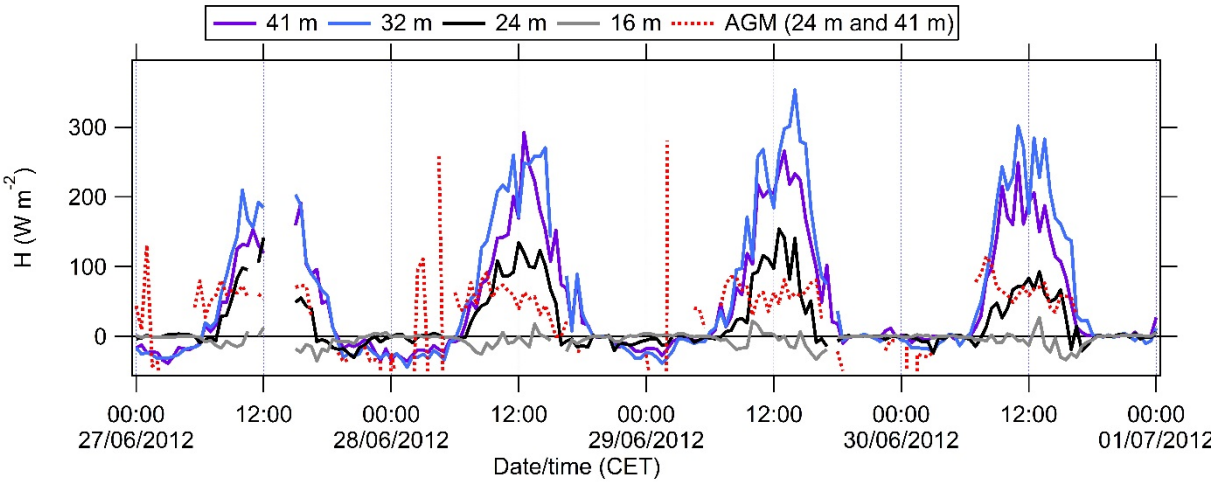

Figure S1. Sensible heat flux measured at Bosco Fontana from the 27/06/12 to 01/07/12. AGM is the aerodynamic gradient method (d=18.67 m), all other measurement heights were by eddy covariance.

A parallel study during the field campaign was taking place as San Pietro Capofiume (SPC), (44°39'N, 11°38'E) Italy, which lies south of Bosco Fontana in the Po Valley. A MARGA instrument was operated at SPC, measuring water soluble inorganic aerosols (NH_4^+, Na^+, K^+, Ca^{2+}, Mg^{2+}, Cl^-, NO_3^- and SO_4^{2-} at both PM_1 and PM_{10}) and their counterpart gas phase (NH_3, HCl, HNO_3, HNO_2, SO_2) at hourly resolution. The method of the MARGA instrument is well described in the literature (Makkonen et al., 2012;Rumsey

et al., 2014;Twigg et al., 2015). The MARGA instrument at SPC used loops and a HNO_3 eluent for the cation column as described by Makkonen et al. (2012). As part of data handling periodic blanks were due to the interference of the HNO_3 eluent, as reported by Makkonen et al. (2012). The average HNO_3/NO_3^- blank was then subtracted from HNO_3 and NO_3^- reported concentrations. Figure S2 presents the measured PM_{10} Cl^- compared with that reported by the GREAGOR at BF. It is evident that Cl^- is of the same magnitude at the two sites and has similar temporal variation. As result the linear regression of Na:Cl at SPC (figure S2) was then used to create a Na^+ time series for BF in order to run the ISORROPIA model II (Fountoukis and Nenes, 2007) by calculating Na^+ from the measured Cl^- at Bosco Fontana.

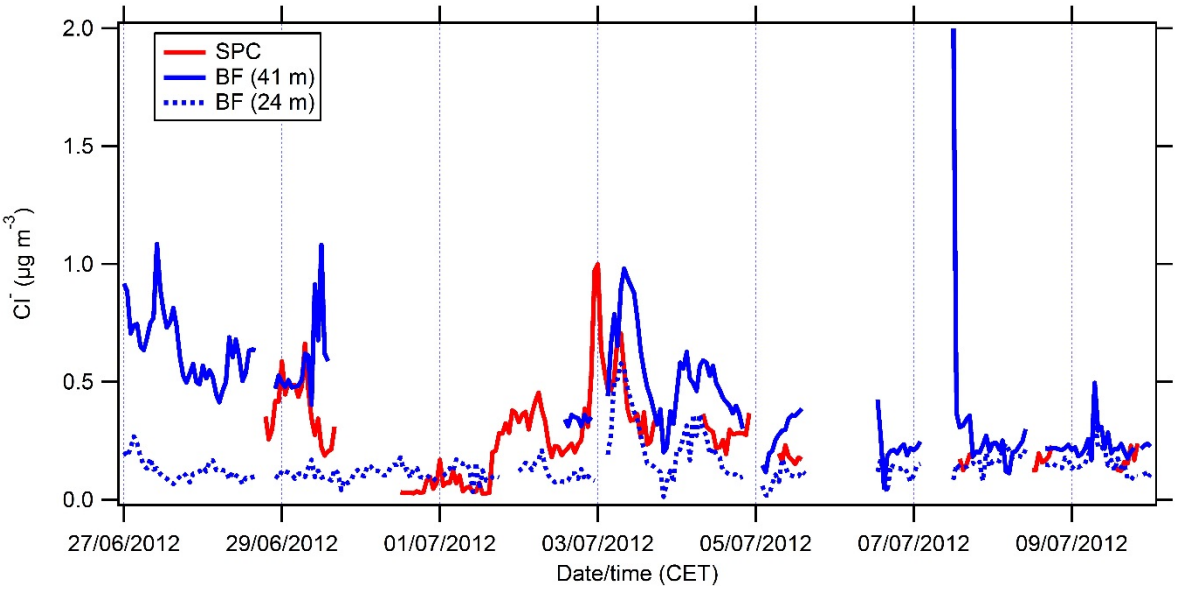

Figure S2 Time series comparing Cl^- measured PM_{10} at San Petro Capiofuime and Bosco Fontana from the 27/06/12 to 10/07/12

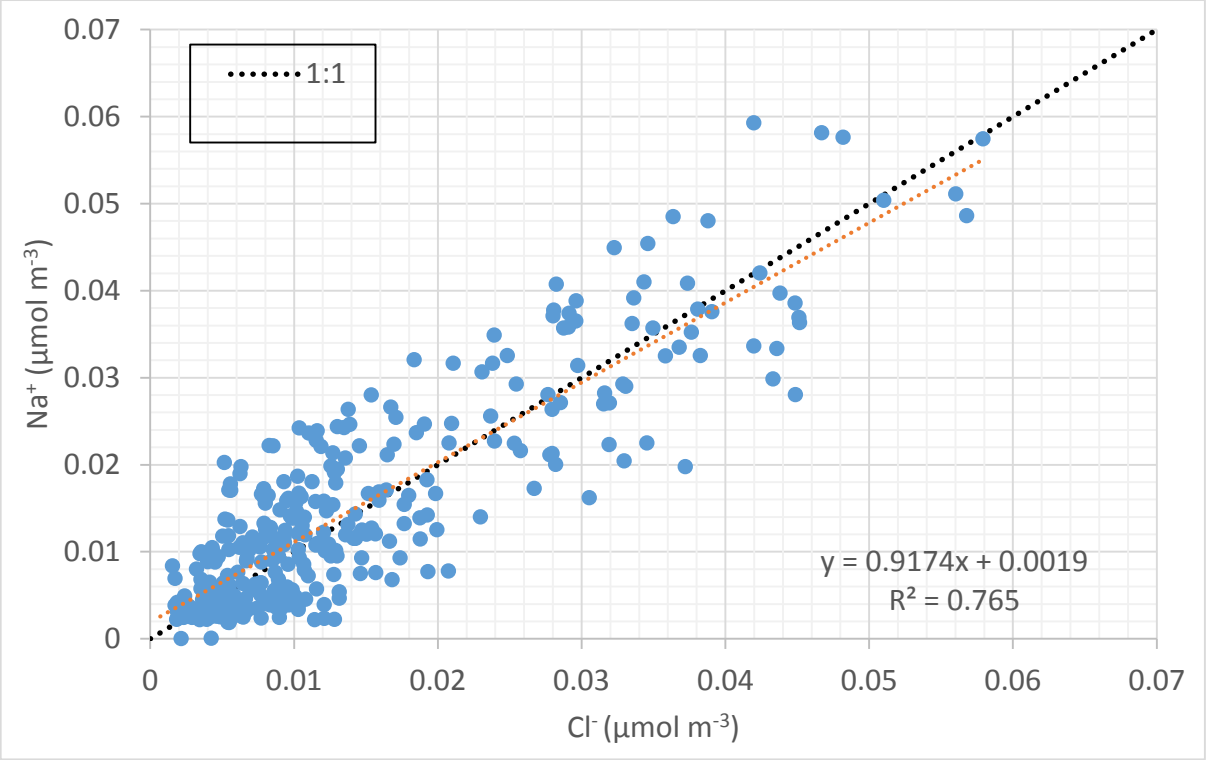

Figure S3. Na:Cl ratio at San Petro Capofiume from the 06/06/12 to 10/07/12.

Ozone fluxes measurements at four levels above, inside and below a forest canopy: interactions with nitrous oxide and implications for the ozone flux partition

Finco, A.[1], Coyle, M.[2]; Marzuoli, R.[1]; Chiesa, M.[1]; Loubet, B.[3]; Diaz-Pines, E.[4]; Gasche, R.[4]; Ammann, C.[5]; Sutton, M.A.[2]; Nemitz, E.[2], Gerosa, G.[1]

[1] Dip. to di Matematica e Fisica, Università Cattolica del S.C., via Musei 41, 25121 Brescia, Italy

[2] NERC Centre for Ecology and Hydrology (CEH), Bush Estate, Penicuik, EH26 0QB, UK.

[3] INRA, UMR 1091-INRA-AgroParisTech, Environnement et Grandes Cultures, 78850 Thiverval-Grignon, France

[4] Institute for Meteorology and Climate Research, Karlsruhe Institute of Technology, Garmisch-Partenkirchen, Germany.

[5] Agroscope Research Station, Climate and Air Pollution Group, Zürich, Switzerland

Abstract

Ozone is detrimental to plants and human health. It is therefore important to develop a robust understanding of how efficiently ozone is deposited to vegetation and to identify the fraction of ozone that enters the stomata where it can cause phytotoxic damage. As part of the FP7 ECLAIRE project an integrated field campaign at the hornbeam-oak forest at Bosco Fontana, Po Valley, Italy, brought together sufficient instrumentation to attribute the O_3 flux to the different pathways. Ozone fluxes were measured at four heights above, within and below the crown space, whilst fluxes of NO were determined at the ground and above the canopy. The O_3 deposition were typically 10 nmol m^{-2} s^{-1} during the day and 2 nmol m^{-2} s^{-1} at night. Soil NO emissions showed little diurnal variability and averaged 76.8 ng N m^{-2} s^{-1}. The detailed results suggest that about 40% of the ozone flux enters the stomata and 30% reacts with NO, based on the difference in the NO flux from the soil and above the canopy. With only 35% of the flux removed by the crown space, it follows that (a) there are stomatal sinks in the understorey, (b) cuticular O_3 deposition in the crown space is insignificant and (c) reaction with NO occurs mainly below the crown layer. The measurements further shed light on the interaction between in-canopy inversion and O_3 exchange.

1. Introduction

Ozone (O_3) has been widely recognized as the most dangerous pollutant for vegetation (Ashmore, 2005; Matyssek and Innes, 1999; Matyssek et al., 2012) and damages to vegetation have been observed from cellular up to ecosystem level (e.g., Dizengremel et al., 2013, Marzuoli et al. 2008). Due to its phytotoxicity, ozone deposition to ecosystems had been widely studied in the last 30 years (e.g. Weslely, 1983; Jacob et al, 1992; Padro,1996; Cieslik, 1998; Lamaud et al., 2001; Mikkelsen et al. 2004, Gerosa et al. 2009, Launiainen et al., 2013) thanks also to the development of fast ozone instruments, suitable for eddy covariance measurements .

First field campaigns were relatively short (e.g. Neumann and den Hartog, 1985,Massman 1992, Cieslik and Labatut 1997) while , with time, longer campaigns (e.g. Mikkelsen et al. 2004, Gerosa et al. 2008, Zona et al., 2014, Fares et al. 2014) lead to a better comprehension of the ozone deposition. Initially it was assumed that ozone deposition was largely controlled by stomatal uptake, whilst non-stomatal deposition was thought be small and almost constant (Colbeck and Harrison, 1985, Fowler, 2009). Since then many studies have demonstrated that non-stomatal deposition is not constant and can be even the major part of the ozone deposition (Cieslik, 2004; Altimir et al., 2004, 2006; Gerosa et al., 2008, 2009; Fowler et al., 2001, Fares et al., 2010; Wesely and Hicks, 2000).

Even if some of the non-stomatal deposition pathways have been studied and quantified, the fate of the ozone deposition below canopy is yet to be completely understood and the contributions to the non-stomatal flux of deposition to leaf surface, deposition to ground and chemical destruction appears to differ greatly between studies. Very few studies measured ozone fluxes above and also below the canopy of a forest (e.g. Launiainen et al., 2013; Fares et al. 2014).

This paper presents results from a joint field campaign, conducted in the context of the ECLAIRE project (FP7). This field campaign took place in the summer of 2012 in a forest in the Po Valley, in northern Italy, and four eddy-covariance systems for ozone were deployed along a vertical profile on a tower: two outside the canopy, one at canopy level and one below canopy. This experimental set-up allowed the fraction of ozone taken up by the canopy to be quantified as a difference between the measurements outside the canopy and the below canopy ones. The combined use of a fast NO analyzer on the top of the tower and of a dynamic chambers system to measure the soil NOx flux allowed to estimate the fraction of the ozone deposition removed by reaction with NO. The dynamics of the ozone and NOx concentrations and fluxes inside and above the forest were investigated as well as their interactions with meteo-climatic drivers in order to improve the comprehension of these phenomena.

2. Materials and methods

2.1 Site characteristics

In the context of the ECLAIRE FP7 European project a joint field campaign was performed at the Bosco Fontana reserve (45°11'52.27"N, 10°44'32.27"E; elevation 25 m asl) located near Marmirolo, Italy. The measuring site is a mixed oak-hornbeam forest, a typical climax ecosystem of the area and it is located just in the middle of the Po Valley, one of the most polluted areas of Europe. The forest is inside a natural oriented reserve classified as a Site of Communitarian Importance and Special Protection Zone (IT20B0011) and it is part of the LTER network.

The dominant tree layer is composed by hornbeam (*Carpinus betulus*, 40.45 % of the total surface of the reserve), oak (*Quercus robur*, 17.09 %), red oak (*Quercus rubra*, 9.65 %) and Turkey oak (*Quercus cerris*, 7.06 %) (Dalponte et al., 2002; Acton et al., 2015). Each of the other species (*Acer campestre, Prunus avium, Fraxinus ornus and oxycarpa, Ulmus minor, and Alnus glutinosa* along the little rivers) accounts for no more than 3% of the total surface. The dominant tree layer is made up by *Corylus avellana*, *Sambuscus* spp, *Cornus mas, Crataegus oxyacantha and monogyna and Sorbus torminalis*, with a dense nemoral layer of butcher's broom (*Ruscus aculeatus*, L)..

The average height of the canopy is 26 m and the average single-sided leaf area index (LAI), measured by a canopy analyser (LAI2000, LiCOR), was 2.28 m^2 m^{-2} with a maximum of 4.22 m^2 m^{-2}.

The soil is a Petrocalcic Palexeralf, loamy skeletal, mixed, mesic (*Campanaro* et al. 2007) according to the USDA classification. The soil depth is 1.5 m with petrocalcic hardened layer between 0.80 and 1 m below the ground; this layer was formed after the gradual lowering of the water table.

The climatic characteristics are typical of the Po Valley, with humid and hot summers and (Longo, 2004). The mean annual temperature is 13.2°C (period 1840-1997; Bellumé et al., 1998), January is the coldest month (1.3°C) while July is the hottest (24.6°C) Annual precipitation is on average 658 mm and May and October are the wettest months on average. A water deficit period generally occurs in July driven by the combination of high temperature and low precipitation. The most frequent wind directions are generally from E and NE, in particular in spring and summer.

2.2 Measurement infrastructure

In order to measure the gas exchange between the forest and the atmosphere, a 40 m tall scaffold tower was mounted inside the forest, with a measuring fetch ranging between a minimum of 390 m in the S direction and a maximum of 1440 m in the NE direction. Four sonic anemometers (see Table 1 for models) were placed on the tower at four different height: 16 m, 24 m, 32 m and 41 m. At the top tower level a LI-COR 7500 (LI-COR, USA) was installed to measure the rapid fluctuations of water and carbon

dioxide density, and at each of the four tower level a fast ozone instrument was installed to measure ozone vertical fluxes. All the fast instruments and the sonic anemometers were sampled at 20 Hz through a customized PC-based data acquisition program (LabVIEW; National Instruments), and the slow sensors were connected to a data logger (CR13X, Campbell Scientific) and sampled once per minute.

2.2.1 Ozone flux measurements

All the fast ozone instruments (see Table 1 for models) are based on the reaction between ozone and a cumarine-47 target which has to be changed after some days because its sensitivity declines exponentially with time (Ermel et al., 2013). Three fast instruments (two COFA and the ROFI) were GFAS clones (Güsten and Heinrich, 1996) equipped with a relatively big fan (about 100 L/min) which led to a faster consumption of the coumarine target than the fourth one, a NOAA prototype (FROM; Bauer et al., 2002), which mounted a small membrane pump (2.5 L/min). For this reason the ozone targets were changed every 5 days for COFA and ROFI and every 10 days for the FROM. In both cases the ozone targets were prepared just before each use by exposing them to a concentration of 100 ppb of ozone for two hours.

Vertical profile of O_3 and NO_x concentrations

A computer controlled switching system of based on Teflon tubing and solenoidal Teflon valves was used to characterize the vertical concentration profile of O_3 and NO/NO_2 above and within the canopy at 5 heights: 8 m, 16 m, 24 m, 32 m and 41 m. The air samples drawn at each level by a 30 L min^{-1} pump were alternately sent to an UV ozone photometer (Thermo Scientific 49C, USA) and to a NO_x chemiluminescence analyser with a thermolytic converter (Thermo Scientific 42C, USA) lodged in an air-conditioned container at the bottom of the tower. The ozone concentrations measured at the 4 uppermost levels were also used as absolute ozone reference for the fast ozone instruments.

2.2.2 Vertical profile of air temperature and humidity and complementary measurements

Four temperature and relative humidity probes (HMP45, Vaisala, Finland), one per each tower level, were mounted to obtain the vertical air temperature and humidity profile, and an additional humitter (HMP45, Vaisala, Finland) was placed at 11 m. A net radiometer NR-lite (Kipp & Zonen, Holland), a BF5 sunshine sensor for total and diffuse PAR (Delta-T Devices, United Kingdom), a PTB101B barometer (Vaisala, Finland) and a rain gauge (mod. 52202, Campbell Scientific, USA) were mounted on the top of the tower.

Several soil probes were deployed in the soil at the bottom of the tower, at a distance of 20 m: four reflectometers for soil water content (TDR mod 616, Campbell Scientific, USA), four soil heat flux plates (mod. HFP01SC, Hukseflux, NL) and four soil temperature probes (PT100, GMRstrumenti, Italy).

2.2.3 NO concentrations and fluxes at 32 m

The NO concentration and fluxes at 32 m were measured using an Ecophysics CLD780TR instrument, based on the chemiluminescence reaction between O_3 and NO. Briefly, O_3 is produced in excess using pure oxygen and injected into a chamber where it reacts with NO producing light which is measured by a highly sensitive photomultiplier cooled at -18°C. The analyser was sub-sampling at 3 L min^{-1} with a 1/8 inch ID PFA Teflon tube of 2 m long out of the main sampling line (3/8 ID Teflon tube, 30 m long with a 60 L min^{-1}) . The analyser was calibrated with a dilution system (LNI 6000x, SW) which was used with a standard NO cylinder (18 ppm) to generate a 80 ppb concentration. The calibration was performed daily at the beginning of the experiment and then weekly. The analyser output was recorded on a computer with another LabVIEW program that insured time alignment with the sonic anemometer.

2.2.4 NO, NO_2 and O_3 flux measurements at soil interface

Fluxes and concentrations of NO, NO_2 and O_3 at the soil-atmosphere interface were determined by use of an fully automated measuring system as described in detail elsewhere (Butterbach-Bahl et al., 1997; Gasche and Papen, 1999; Rosenkranz et al., 2006; Wu et al., 2010). Briefly, five dynamic measuring chambers and one dynamic reference chamber were installed at the site. Dimensions of the chambers were: 0.5 m x 0.5 m x 0.15 m (length x width x height). In contrast to the measuring chambers, the reference chamber was sealed gastight against the soil surface using a perspex plate. The time resolution for flux measurements was 1 hour, where every chamber was closed and measured for 6 minutes, and before every sampling of a measuring chamber the reference chamber was sampled, resulting in a measuring cycle of 60 minutes. Within each 6 minutes sampling time concentrations of NO, NO_2 and O_3 were determined two times each. During sampling ambient air was sucked at a constant rate of 50 L min^{-1} across the surface of the chambers and transported via PTFE tubings (inner diameter: 10 mm, length 20 m) to the analyzers. NO and NO_2 concentrations were determined using a chemiluminescence detector CLD 770 AL and a photolysis converter PLC 760, both Eco Physics AG, Dürnten, Switzerland. Ozone concentrations were determined using an infrared ozone analyzer (TE49C, Thermo Environmental Instruments Inc., Franklin, Massachusetts, United States). Corrections for initial concentrations of NO, NO_2 and O_3 at the outlet of each chambers and calculation of fluxes of NO and NO_2 was performed according to Butterbach-Bahl et al. (1997). Calibration of the chemiluminescence detector was performed at least weekly using 40 ppb NO in synthetic air produced by dilution of standard gas (4 ppm NO in N_2) with synthetic air (80% N_2, 20% O_2, both gases Air-Liquide, Kornwestheim, Germany) using a computerized multi gas calibrator (Model 6100, Environics Inc., West-Wellington, United States). Efficiency of photolytic conversion of NO_2 to NO was determined at least weekly as described in detail by Butterbach-Bahl et al. (1997).

2.3 Measuring period

The measuring campaign began on 12th June and ended one month later, on 11th July 2012. From the 12th June to the 23h June three fast ozone instruments (ROFI, FROM and one of the two COFA) were placed above the canopy at 32 m height and were ran in parallel in order to establish the level of their agreement and to characterize their performances (intercomparison period). The COFA installed at the top of the tower started its measurements on 12th June and was not moved to level 32 m for the intercomparison because it was already calibrated against the second COFA.

The 24th June each fast ozone instrument was moved to a different level (Table 1) to begin the flux profile measurements which ended the 11th July (Flux Profile period).

2.4 Data processing

The flux measurement technique adopted was the eddy covariance (e.g. Foken, 2000) which derives the flux as the covariance between the vertical wind component and the scalar of interest: temperature for sensible heat fluxes, absolute humidity for evaporation/latent heat fluxes, ozone concentrations for the ozone fluxes. Hence, these fluxes are described by the following equations:

$$F O_3 = \overline{w' O_3'} \quad (1)$$

$$H = \rho c_p \overline{w' T'} \quad (2)$$

$$LE = \lambda \rho \overline{w' q'} \quad (3)$$

$$F NO = \overline{w' NO'} \quad (4)$$

where w is the vertical component of the wind vector, O_3 is the ozone concentration, ρ is the air density, c_p is the specific heat at a constant pressure, T is the air temperature, λ is the latent heat of vaporization and q is the specific humidity. Primed quantities represent the fluctuations around their mean, indicated by the overscript bars (pal Arya, 1988). An averaging period of 30 minutes was used for the calculation of the means.

The data treatments described hereafter were performed sequentially on the data in order to get to correct flux calculations.

1. *Despiking.* The data series were divided into 2-minute sub-series and for each of them block average and standard deviation were calculated. Spikes were identified as the instantaneous data that differed from the average of each sub-series by more than 3.5 times the standard deviation, as proposed by Vickers and Mahrt (1997). Spikes were removed from the series and the data were than gap-filled by linear interpolation.

2. *Rotations.* Two instantaneous rotations were applied: the first one to align the horizontal wind to the average *u* component recorded in the half an hour ($\bar{v} = 0$), and the second one to rotate the *xy* plane in order to zero the average vertical component of the wind ($\overline{w} = 0$) (McMillen, 1988; Wilczak et al. 2001). This corrected the little imperfections in the sonic anemometers vertical alignment and prepare the data for flux calculations. Periods with a second rotation (vertical) angle greater than 15° were discarded.
3. *Linear detrending*. The fluctuations of each parameter (e.g. *w'*, *T'*, O_3') were calculated as the differences of each instantaneous value from the best linear fit (minimum square) of the considered time series in each half an hour data (Lee at al., 2004). No block averaging or recursive filter were used.
4. *Time-lag determination.* Ozone fluxes have been calculated using a fixed time-lag between the vertical wind and the ozone concentration time series. The lag of each fast instrument was determined by searching for the absolute maximum of the cross-covariance function between the vertical component of the wind and the ozone concentrations at each tower level. Then the time lag to be applied to each instrument (characteristic time-lag) was chosen as the most frequent one displayed by that instrument.
5. *Elimination of the ozone fluxes below the flux error threshold.* The flux error threshold was quantified for each semi-hourly data series by following the methodology proposed by Langford et al. (2015). The standard deviation of the auto-correlation function was calculated for each semi hourly data, with lags ranging between 30 and 60 seconds from the characteristic time lag of each instrument. Fluxes lower than the 95th percentile of the standard deviation were discarded.
6. *Frequency loss correction.* The frequency loss correction factors for the different fast ozone instruments were identified by calculating the co-spectra between *w* and O_3 and by performing an ogive analysis according to Amman (2006).The ogives are the cumulative co-spectra over all the frequencies, and they were calculated and normalized to 1 both for ozone and sensible heat fluxes. The correction factor for each fast ozone analyzer was obtained by normalizing the ozone flux ogive to the sensible heat ogive at low frequencies (up to 0.0065 Hz), and then calculating the ratio between the sensible heat and the ozone ogives one at high frequencies.
7. *Schotanus and WPL corrections*. H, LE and trace gas fluxes were corrected for air density fluctuations. The formulation adopted for the correction of H was the one proposed by Schotanus et al. (1983) while the formulation used for LE and trace gases was the one proposed by Webb et al. (1980).

Fast-response dry chemiluminescence analysers are not absolute instruments, because the sensitivity of the coumarine targets declines with time. Thus, the fast ozone concentration data (acquired as voltages) required additional processing for the calculation of ozone fluxes in physical units.

First of all, the target zero V_0 (Muller et al., 2010)– i.e. the output voltage of each fast ozone instrument at zero ozone concentration – was identified per each coumarine target employed. Then the ozone fluxes were calculated by the following equation (Muller et al. 2010):

$$F_{O3}=\frac{\overline{w'V'}}{\bar{V}-V_0}O_3 \quad (5)$$

$$F_{NO}=\frac{\overline{w'cps'}}{cps-cps_0}S_{NO} \quad (6)$$

where $\overline{w'V'}$ is the covariance between the vertical wind component and the raw output voltage of the fast ozone instrument, $\bar{V}$ is the average output voltage of the instrument in each half an hour, V_0 is the target zero identified for that half an hour, and O_3 is the ozone concentration measured by the reference ozone analyzer during the same period; cps is the NO raw data measurement and cps_0 and S_{NO} are the offset and sensitivity of the fast NO analyser determined during its calibration. The value of *cps0* ranged from 1000 to 2500 cps (counts per seconds) while S_{NO} ranged from 10000 to 12000 cps / (µmol m^{-3}).

In order to avoid a divergence of the denominator in Eq. (4), data with $\bar{V}$ differing from V_0 less than 15% were discarded. This situation happened typically in the first hours of the day when ozone concentrations were low. Again, the data of two hours following each target change were excluded in order to let the target sensitivity to stabilize after the target installation.

Finally, the stationarity of the data was verified as Foken and Wichura (1996) proposed and the non-stationary data were discarded.

Table 1. Instrumentation used at each level on the tower

Level / Height (m)	Ultrasonic anemometer	Fast ozone analyzer	Other fast analyzer	Slow sensors
41	USA1 (Metek)	COFA (Ecometrics)	LI-COR 7500 (CO_2/H_2O)	Vaisala HMP45, Finland NR-lite (Kipp & Zonen, Holland BF5 (Delta-T Devices, United Kingdom) PTB101B (Vaisala, Finland) rain gauge (mod. 52202, Campbell Scientific, USA)
32	HS50 (Gill)	ROFI (CEH)	Ecophysics CLD780TR	Vaisala HMP45, Finland
24	Windmaster PRO (Gill)	FROM (NOAA)	-	Vaisala HMP45, Finland
16	Windmaster PRO (Gill)	COFA (Ecometrics)	-	Vaisala HMP45, Finland
11				Vaisala HMP45, Finland
Soil				TDR mod 616, Campbell Scientific, USA HFP01SC, Hukseflux, NL PT100, GMRstrumenti, Italy

3. RESULTS

3.1 Meteorological conditions during the campaign

Some severe rainfalls cooled air before the beginning of the field campaign so that, air temperature increased significantly in the first days and after that remained stable (Figure 1). The average temperature at the top of the tower was 25.9 °C while the average temperature at 11 m was one degree less (24.9 °C). The maximum temperature during the whole period was 36.2 °C which was observed at the top canopy level (24 m).

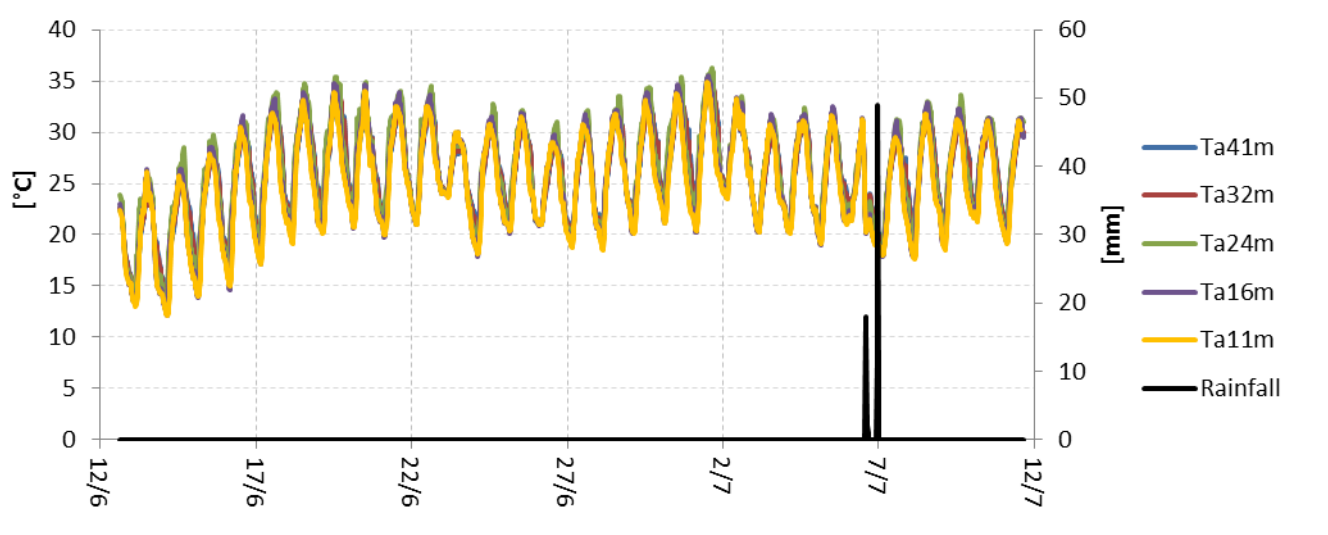

Figure 1. Temperature evolution at the five levels (blue line refers to 41 m, red line to 32 m, green line to 24 m, purple line to 16 m and yellow line to 11 m). Black line are rainfalls.

On average the temperature minimum was observed during night at around 3:00 (Figure 2) for the in-canopy levels (11 m, 16 m and 24 m) and one hour later for the upper levels, with values ranging from 19 °C to 21 °C. Only two significant rainfall events occurred in the final part of the campaign accounting for 108 mm of rain but did not affect significantly air temperature.

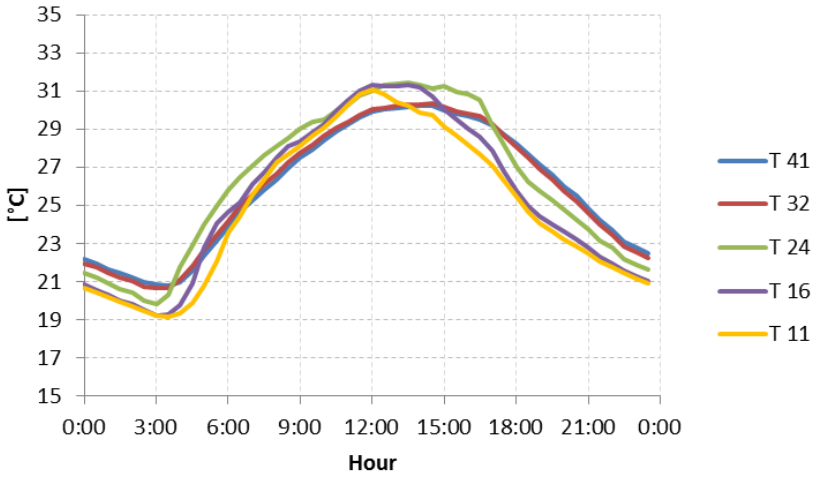

Figure 2. Average daily course of air temperature at the five levels (blue line refers to 41 m, red line to 32 m, green line to 24 m, purple line to 16 m and yellow line to 11 m).

In general most of the days were sunny (only three days were partially clouded) and relatively humid, with nighttime peaks of relative humidity of up to 80% (on average) and daily minima around 40%; a progressive increase of relative humidity in the lower levels was observed from 9:00 hrs (Figure 3).

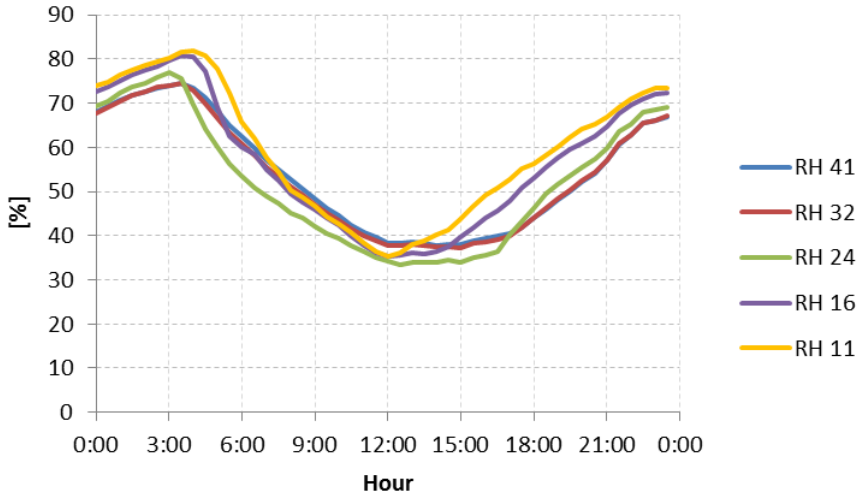

Figure 3. Average daily course of air relative humidity at the five levels (blue line refers to 41 m, red line to 32 m, green line to 24 m, purple line to 16 m and yellow line to 11 m).

The measuring site was characterized by a wind blowing mostly on the west-east direction, with about 50% of the data in this direction (Figure 4), while north-south direction accounted for 12% of the data and the intermediate directions accounted for less than 20% of the data.

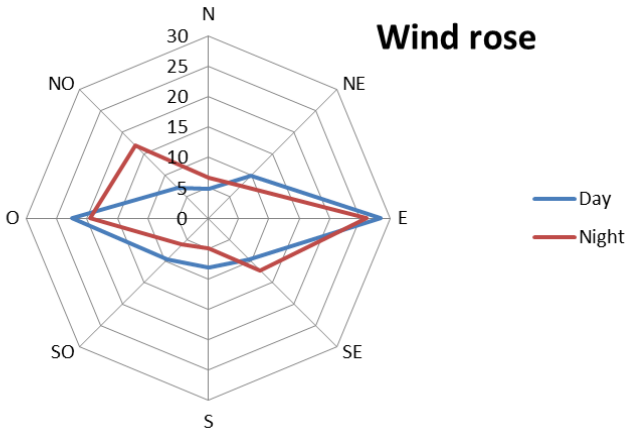

Figure 4. Wind rose based on 41 m data, the radial axis unit indicates the percentage of the data in each direction, the blue line diurnal data, the red line nighttime data.

Windspeed at 41 and 32 m averaged about 2.0 and 1.5 m s^{-1}, respectively (Figure 5), with slightly larger values during night than during day, nearly 1 m s^{-1} more at 41 m and 0.5 m s^{-1} at 32 m. The two lower levels showed very low wind speeds, below 0.5 m s^{-1}, with a minor increase during the day.

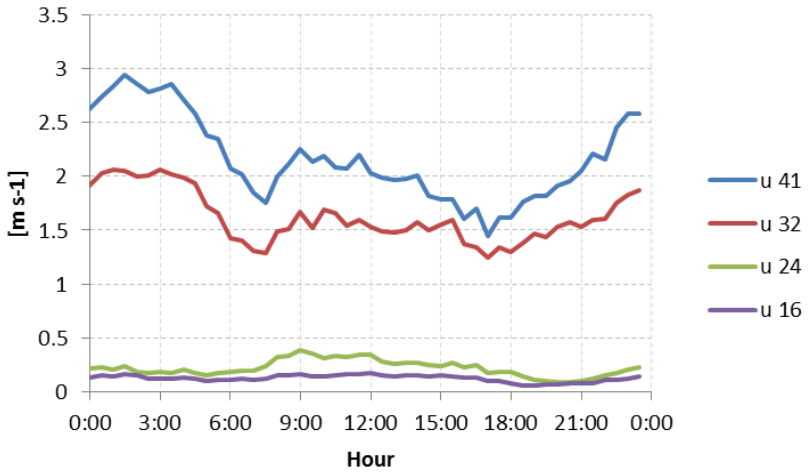

Figure 5. Average daily course of wind intensity at the four levels (blue line refers to 41 m, red line to 32 m, green line to 24 m and purple line to 16 m).

The friction velocity at the two upper levels above the canopy showed very similar behavior (Figure 6) and was slightly higher at 32 m, however the difference between them is less than 10% as expected for the constant flux hypothesis (Foken, 2000). Daily maximum was about 0.5 m s^{-1}, just before noon, and the minimum (0.13 m s^{-1}) was observed around 20:00 and then showing a quite irregular behavior during the night, with values between 0.2 and 0.3 m s^{-1}. In-canopy measurements of friction velocity showed less variability during night, with values below 0.1 m s^{-1}, and the daily maxima, around noon, was 0.25 m s^{-1} at 24 m and 0.18 m s^{-1} at 16 m.

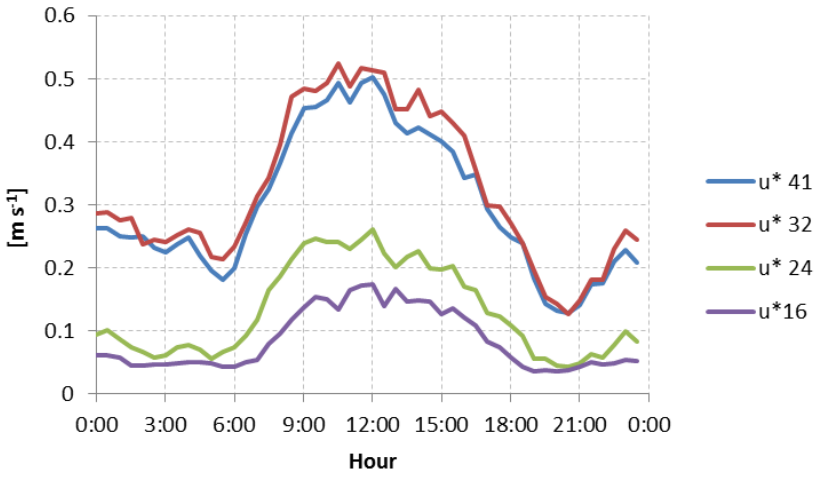

Figure 6. Average daily course of friction velocity at the fourl levels (blue line refers to 41 m, red line to 32 m, green line to 24 m and purple line to 16 m).

3.2 Development of in-canopy thermal inversion, heat fluxes and atmospheric stability

Since the sunrise, early in the morning, the heating of the top part of the canopy developed a thermal inversion into the forest with the ceiling at the top of canopy (level 24 m) and the base at ground level (Figure 7).

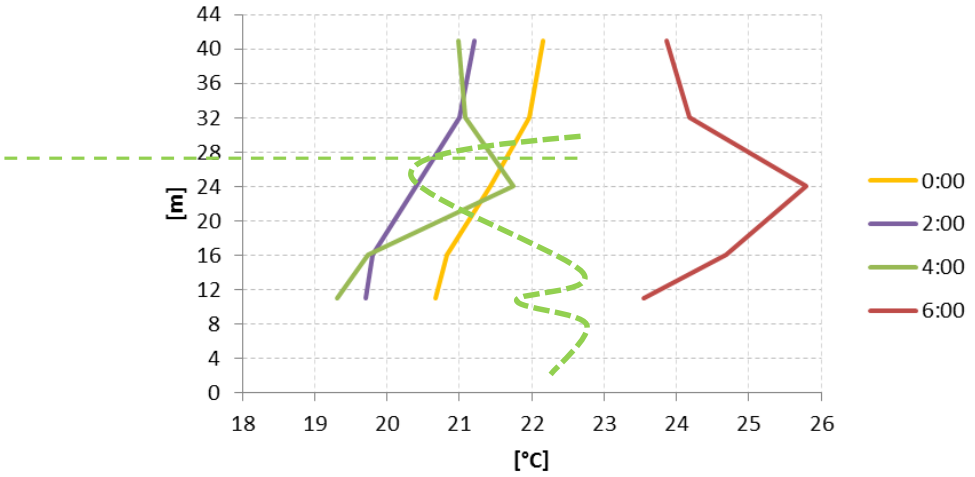

Figure 7. Evolution of the vertical temperature profile over the first hours of the day: the yellow line refers to 0:00 AM measurements, the purple line to 2:00, the green line to 4:00, the red line to 6:00. The green dashed line represents the canopy distribution.

At noon, due to the heating of the whole canopy, this inversion was temporarily depressed and the ceiling was lowered to the bottom part of the tree crowns (level 16 m). But already from 2 pm the inversion

reactivated its top crown ceiling and gradually became more intense during the afternoon because of the cooling of the lower air layers (Figure 8). At 6 pm the inversion is so intense that it reaches the above canopy levels, then it attenuated overnight, without ever disappearing.

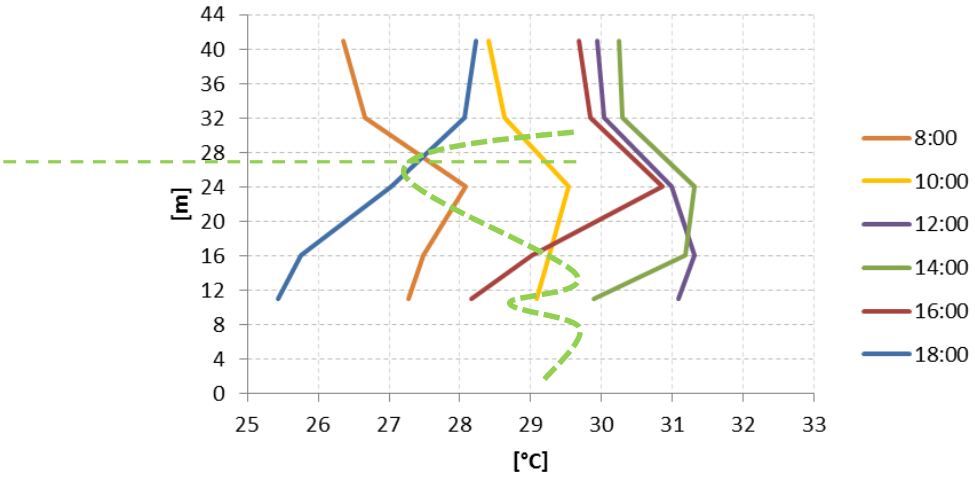

Figure 8. Temperature profile evolution in the central hours of the day: the yellow line refers to 10:00 AM measurements, the purple line to 12:00, the green line to 14:00, the red line to 16:00 and the blue line to 18:00. The green dashed line represents the canopy distribution.

The presence of an inside canopy thermal inversion is confirmed also by the measured sensible heat fluxes (Figure 9) Above the canopy the heat fluxes were strongly upward during the day, while at the top of the canopy (level 24 m) these upward fluxes were much less intense than above (less than half the above canopy ones). By contrast, the below canopy heat fluxes were almost always zero or downward headed (cf. level 16 m). In relation to the strengthen of the thermal inversion in the afternoon, it is worth noting that downward heat fluxes were recorded at 16 m starting from 2 pm, and from two hours later at the 24 m level. However, the forest released most of the energy as latent heat with a peak around 300 W m^{-2} after midday and with near-zero nighttime values.

Above the canopy the atmosphere was nearly always unstable during the day, whilst below canopy it was mostly stable, as showed in Figure 10. At the top canopy level (24 m) the stability was most frequent early in the morning and, remarkably, during the inversion and it strengthened from 3 pm to 7 pm. During the night the atmosphere was mainly stable or very stable above canopy, while in the two lowermost levels it was observed some nocturnal instability.

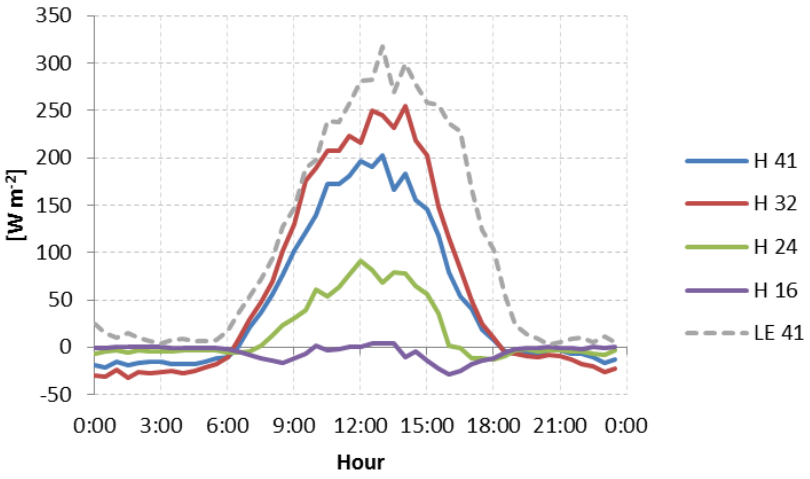

Figure 9. Average daily course of sensible heat fluxes at the four levels (blue line refers to 41 m, red line to 32 m, green line to 24 m, purple line to 16 m), dashed grey line is the latent heat flux measured at 41 m.

a) 41 m

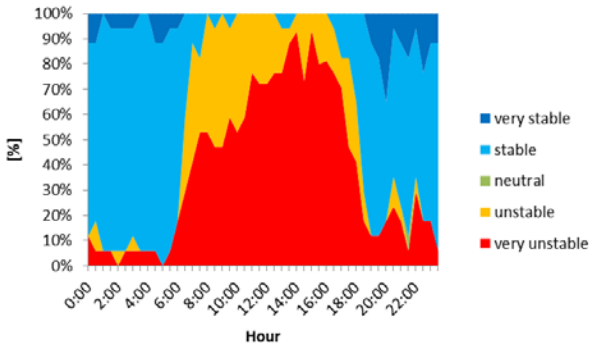

b) 32 m

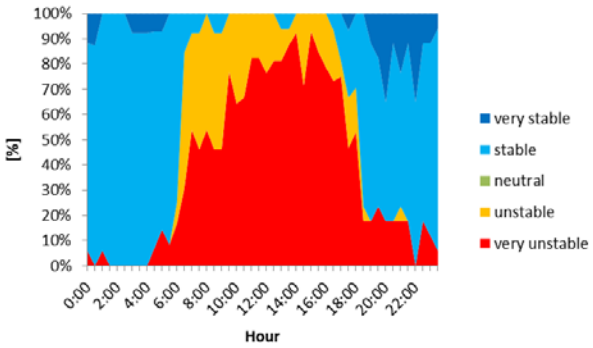

c) 24 m

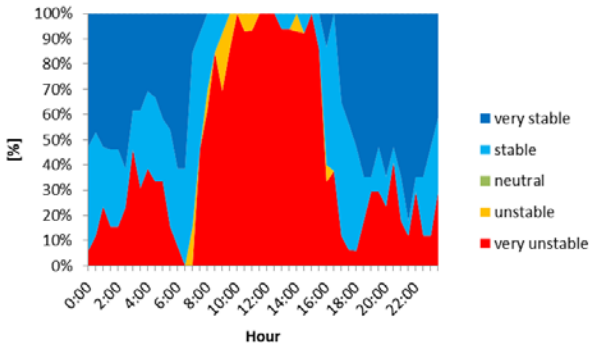

d) 16 m

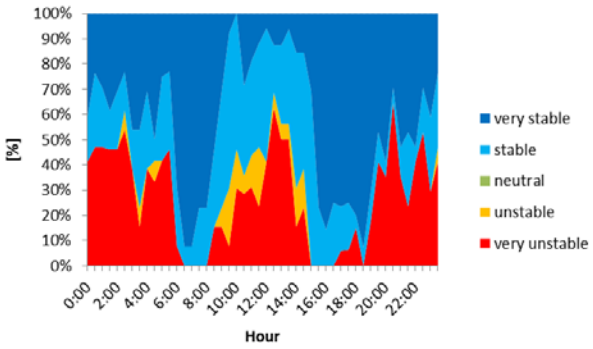

Figure 10. Stability class distribution expressed as function of the stability parameter ((*z*-*d*)/*L*), where *z* is the measuring height, *d* is the zero-plane displacement height and *L* the Obukhov length.

3.3 Ozone concentrations profiles

The ozone concentration profile was almost constant during night and the morning from 8 to 41 m (Figure 11) but, after midday, a peak was observed at the 32 m until 16:00 and also at 24 m, although less intense and for a shorter period. Moreover, in the afternoon, from 15:00 to 18:00 a remarkable decrease at the lowest level (0.15 m) was observed (Figure 11). Vertical ozone concentration profiles (Figure 12 and Figure 13) showed a possible ozone formation above canopy (level 32) from late in the morning until early in the evening.

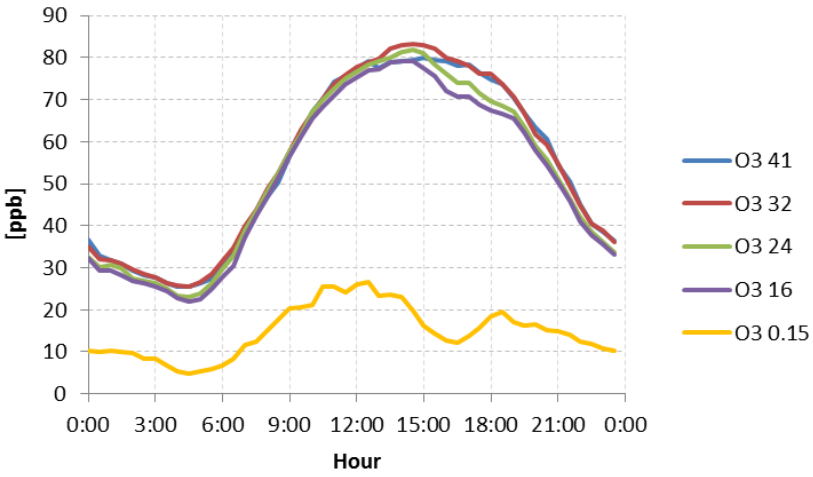

Figure 11. Ozone concentrations at the five levels (blue line refers to 41 m, red line to 32 m, green line to 24 m, purple line to 16 m and yellow line to 0.15 m).

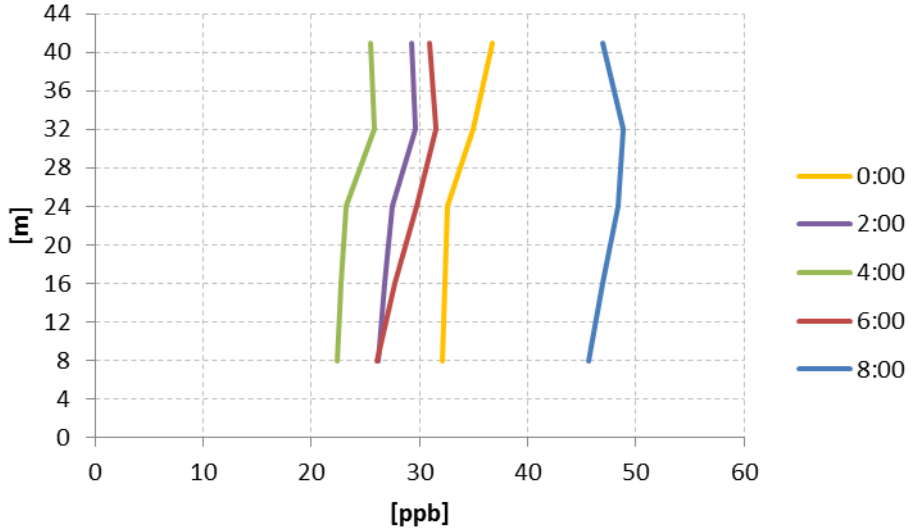

Figure 12. Ozone concentration profile evolution in the central hours of the day: the yellow line refers to 0:00 AM measurements, the purple line to 2:00, the green line to 4:00, the red line to 6:00 and the blue line to 8:00.The 0.15 m level has not been included here for clarity.

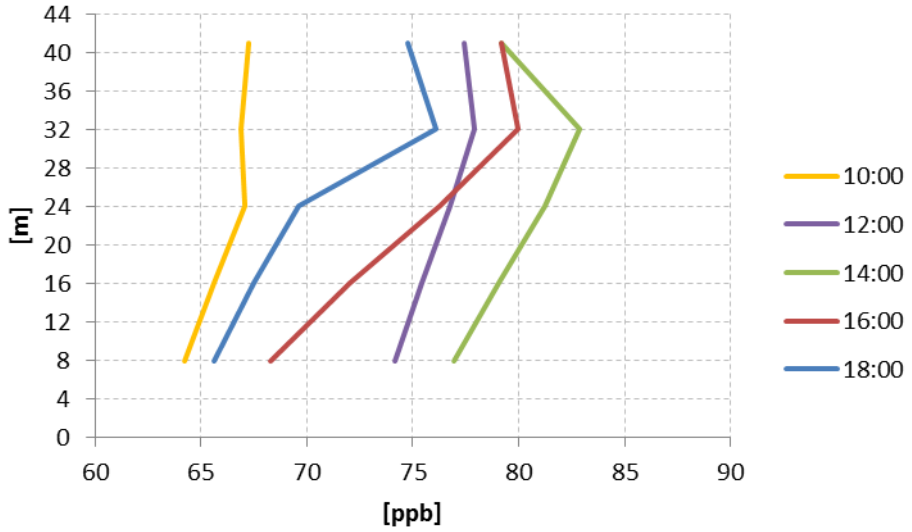

Figure 13. Ozone concentration profile evolution in the central hours of the day: the yellow line refers to 10:00 AM measurements, the purple line to 12:00, the green line to 14:00, the red line to 16:00 and the blue line to 18:00. The 0.15 m level has not been included here for clarity.

An ozone consumption below canopy was observed already in the morning at 16 m and from midday also at 24 m. From 13:00 to 15:00 greater ozone concentrations were observed above canopy (at 32 m and, to a lesser extent, at 24 m), thus strengthening the hypothesis of a local production of ozone. In the afternoon the ozone consumption below canopy was even greater leading to larger differences between the 32 m and the 16 m levels.

3.4 NO and NO_2 fluxes and concentrations

NO and NO_2 fluxes at ground level were almost always mono-directional with NO emitted from soil emission and NO_2 deposited to the ground. A significant change in the emission rate of NO and in the deposition of NO_2 was observed after the rainfalls happened during the night between 6th and 7th July (Figure 14).

The average daily course of soil fluxes showed an almost constant emission of NO with two decreases: one around 6:00 and the other 16:00 (Figure 15), both of them happened just after O_3 decreases at 0.15 m (Figure 11).

Both NO and NO_2 concentrations did not show great difference along the vertical profile (Figure 16 and Figure 17). The greatest differences between the bottom and top level were only around 1 ppb, for both compounds, very early in the morning, between 4:00 and 6:00.

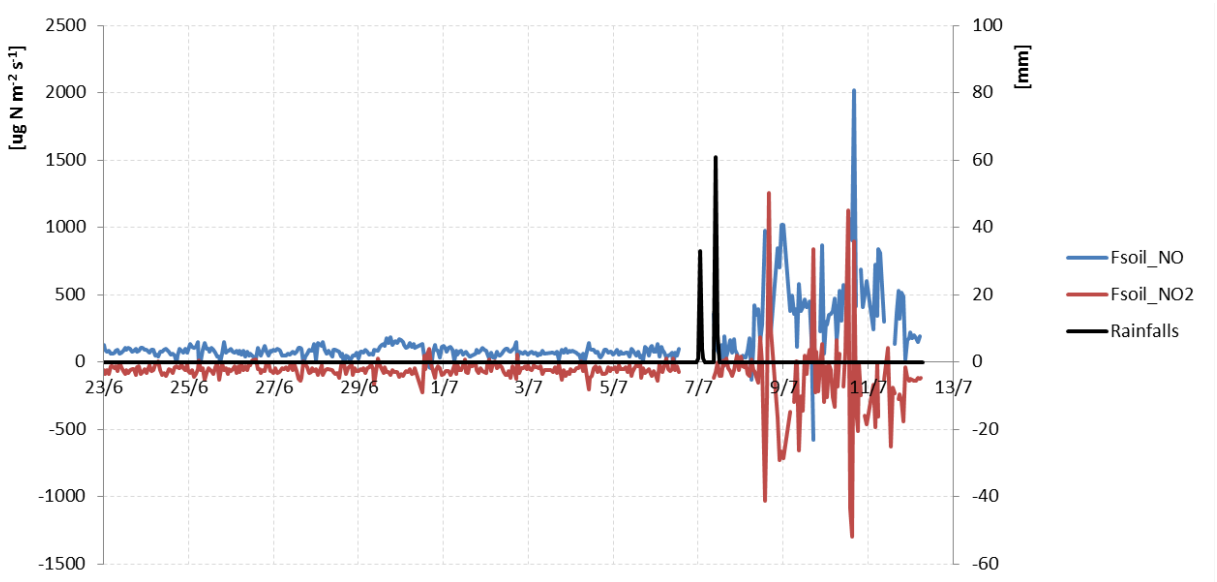

Figure 14. NO and NO_2 soil emissions in the profile period (blue and red line respectively) and rainfalls (black line)

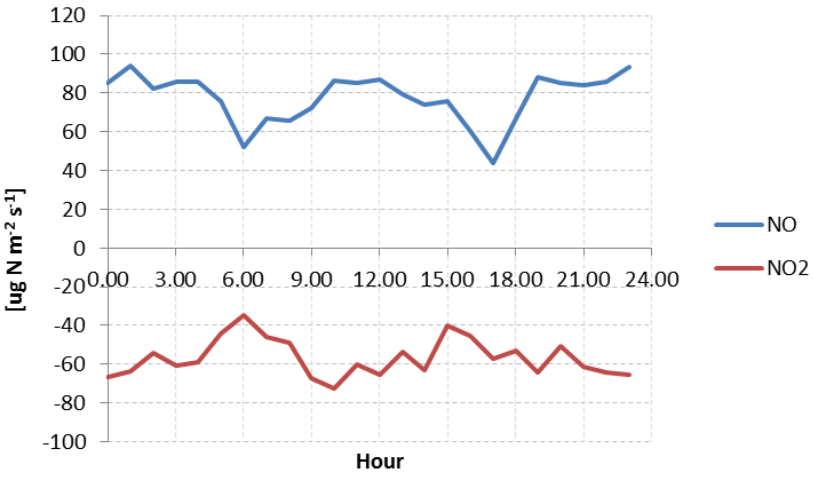

Figure 15. Average daily course of soil NO (blue line) and NO_2 fluxes (red line). Data after rainfalls have been excluded.

The NO concentrations measured at 32 m with the fast Ecophysics instrument were in agreement with the profile measurements with low concentrations ranging from 0 to 7 ppb (0-0.3 µmol m^{-3}), but was most of the time below 0.5 ppb. The NO flux was mostly directed towards deposition. Both NO concentrations and fluxes at 32 m showed a clear diurnal pattern, with NO concentration peaking in the morning at around 7:00 while the NO flux was peaking at around 8:00 in the morning. After 12:00 the flux and concentrations were both very small. No afternoon NO traffic peak was observed. This pattern is entirely consistent with the measurement performed with the "slow" analyzers on the profile, although the concentration is a bit lower on average (Figure 18).

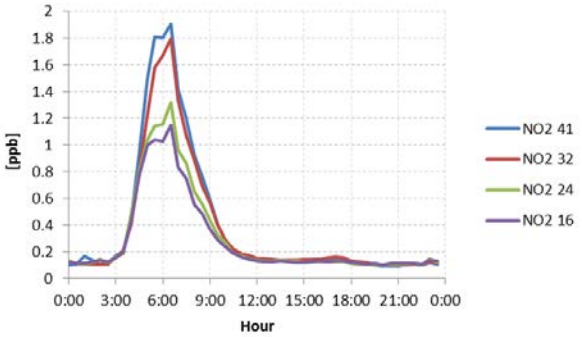

Figure 16. NO concentrations at the four levels (blue line refers to 41 m, red line to 32 m, green line to 24 m, purple line to 16 m).

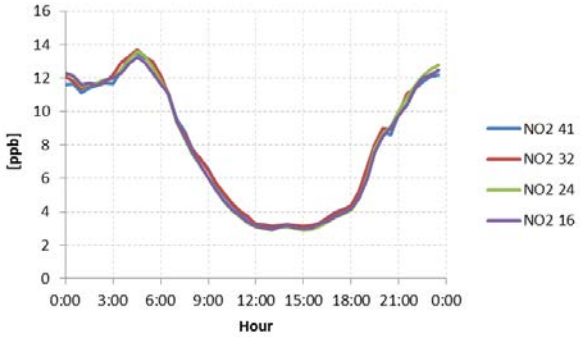

Figure 17. NO_2 concentrations at the four levels (blue line refers to 41 m, red line to 32 m, green line to 24 m, purple line to 16 m).

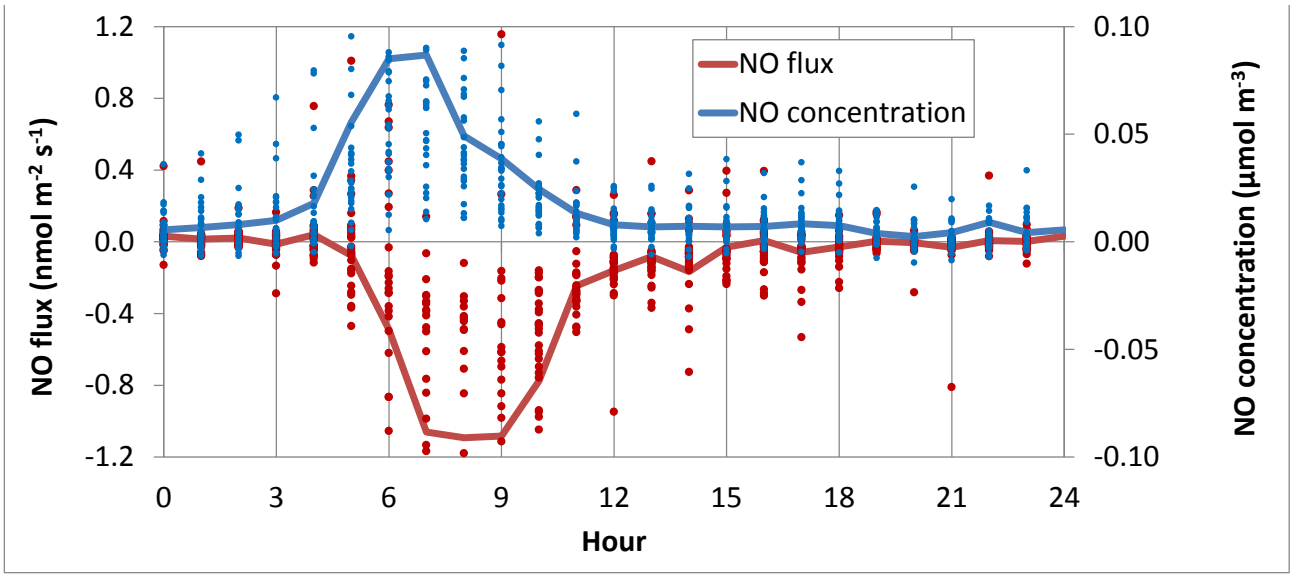

Figure 18. Daily pattern of the NO concentration and fluxes measured at 32 m with the Ecophysics CLD780TR and the eddy-covariance method. Points shows the individual data, while lines show the hourly averages. The scale has been magnified for clarity sake, hence each individual point are not shown on the graph.

3.5 Ozone fluxes profile

In order to calculate ozone fluxes the characteristic time lag of each instruments had been found. The instruments deployed inside the canopy (FROM and one of the two COFA) showed different lags in the co-sampling and in the profile period. For instance, Figure 19 shows the lag distribution of the FROM with a lag equal to 4.6 s in the co-sampling period and to 8.3 s during the profile period. Similar results were obtained for the COFA placed at 16 m (lag = 1.0 s in the co-sampling period and 11.4 seconds in the profile period). Since the lag is due to physical characteristics of the instrument and in particular it should be equal to the time for the air transit from the inlet to the photomultiplier, the choice of lag was based on the co-sampling period data, that is when the instrument was working in normal conditions outside the canopy. For the same reason also the frequency loss corrections were based only on the co-sampling period data. Data of both these corrections can be found in Table 2. The three instruments running at 32 m during the co-sampling showed a quite good agreement, in Figure 20 the deposition velocity measured by the three instruments can be found.

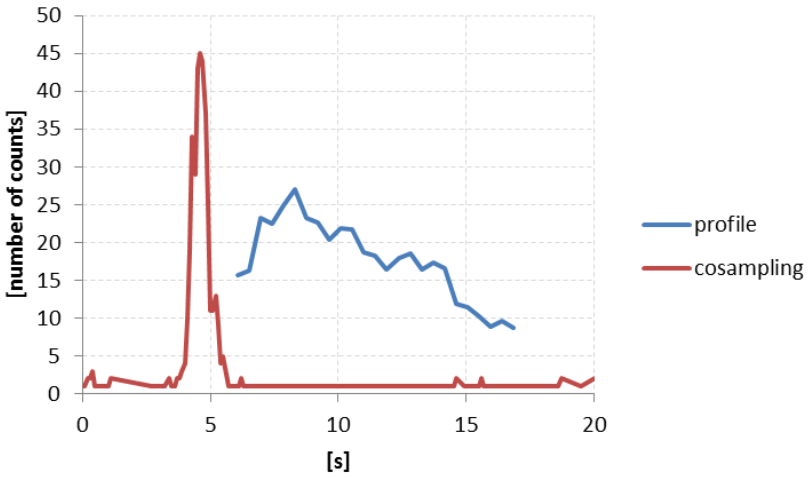

Figure 19. Lag distribution of the FROM instrument in the two measuring period

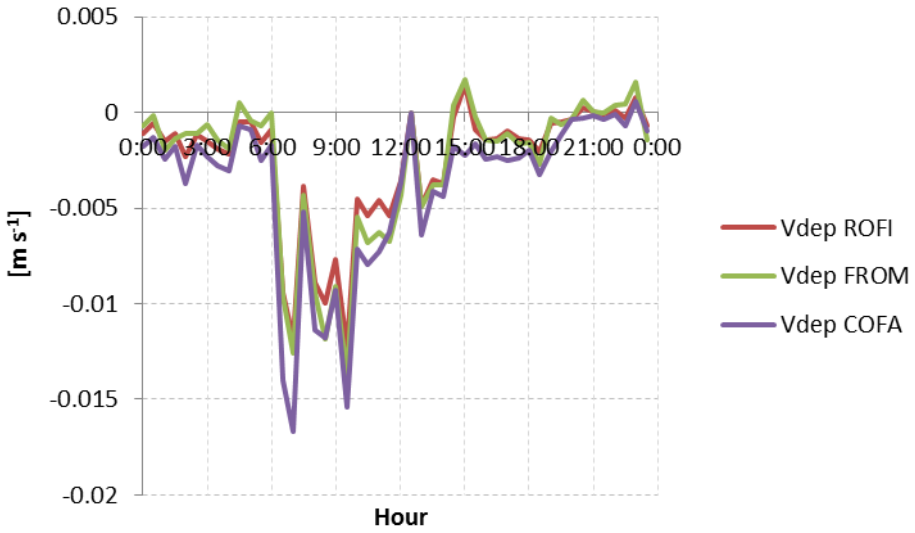

Figure 20. Deposition velocity of the three instruments deployed at 32 m during the co-sampling period

Table 2. Characteristic time lag in both periods (co-sampling and profile) and frequency loss corrections for the fast ozone analyzers.

Instrument and height	Lag (co-sampling period) [s]	Lag (profile period) [s]	Frequency loss correction [%]
COFA 41 m	0.75	-	+1
ROFI 32 m	1.3	-	+2
FROM 24 m	4.6	8.3	+15
COFA 16 m	1	11.4	+6

Ozone fluxes showed a regular behavior with almost negative values except rare positive peaks almost during night or during the transition between night and day (Figure 21) while, in the central hours of the day, they were around 10 nmol m^{-2} s^{-1} for the two upper levels (slightly greater at 32 m), higher for the 24 m level (12 nmol m^{-2} s^{-1}) and lower for the below canopy level (16 m) with 6 nmol m^{-2} s^{-1}. The highest deposition rates were observed on 26th June at the top level with 41 nmol m^{-2} s^{-1} at the 41 m level. In general, ozone fluxes at all four levels started to increase after 7:00 in agreement with the increase of friction velocity (Figure 22 and Figure 6) and reached their maximum around 9:00, remained nearly stable unitl 14:00. After 14:00, a decrease of fluxes can be observed first at 24 m and after 16:00 at all the other three levels. Typical nighttime values of below 2 nmol m^{-2} s^{-1} were reached at 19:00, slightly higher nighttime fluxes were observed at 41 m values.

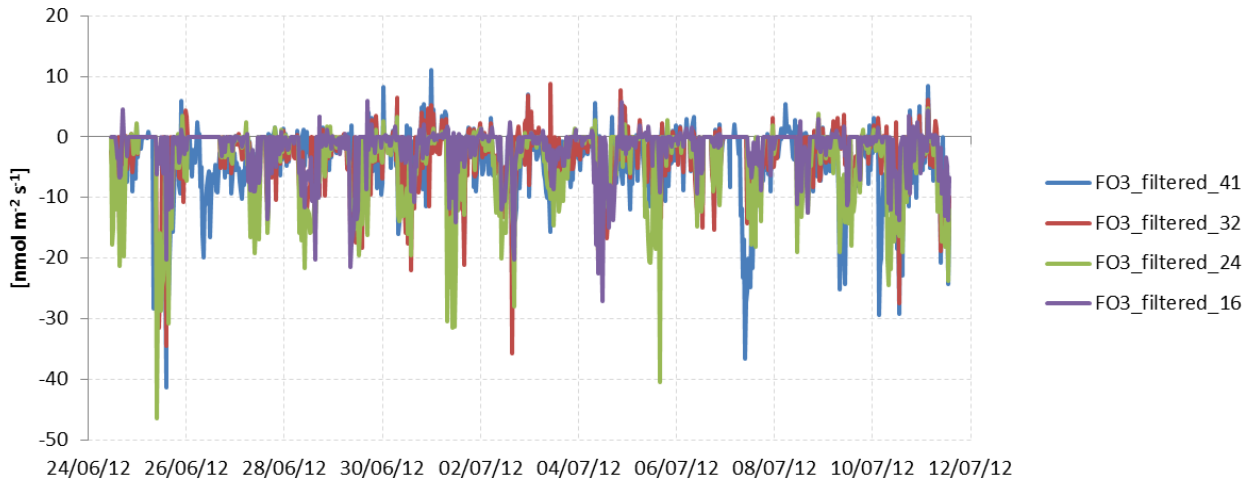

Figure 21. Ozone fluxes evolution at the four levels (blue line refers to 41 m, red line to 32 m, green line to 24 m, purple line to 16 m and yellow line to 11 m).

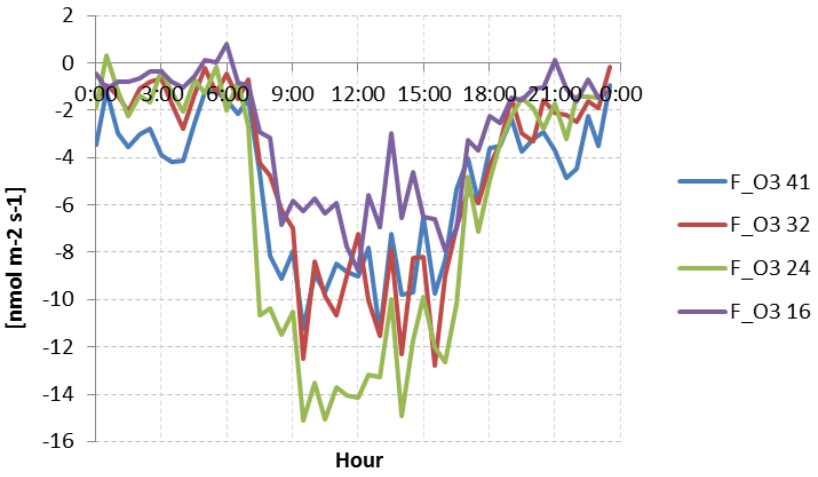

Figure 22. Average daily course of sensible heat fluxes at the four levels (blue line refers to 41 m, red line to 32 m, green line to 24 m, purple line to 16 m),

4. Discussion

Bosco Fontana forest was characterized by a strong thermal inversion below canopy (Figure 7 and Figure 8) which, in the end, affected the gas exchange between the forest and the atmosphere. Diurnal inversion is a relatively known feature: sunlight irradiates and heats leaves, leading to a heating of the canopy and the surrounding air. As a consequence the typical profile of temperature shows a diurnal maximum at canopy height and more pronounced minimum during night (Monteith and Unsworth, 2014). In forests, in particular in those with relatively open canopies and ventilation, temperature gradients are in general low (Pal Arya, 2001; Launiainen, 2011).

At Bosco Fontana the lower layer (11-16 m) was always under thermal inversion and only in the central hours of the day (10:00 – 14:00) did the thermal inversion extend also to the entire canopy, up to the 24 m level. The presence of a quite constant thermal inversion resulted in the division of the studied aerological domain in two vertical regions: an above canopy one and a below canopy one. Nighttime temperature gradients were always positive (increasing with increasing heights) with no evidence for a minimum at the crown level. In general, temperature gradients measured here were steeper than many other measurements found in literature (e.g. Utiyama et al., 2003; Pal Arya, 2001; Launiainen, 2011). The density of the trees and of their canopy might have affected the temperature profile, not allowing the radiation to heat enough the forest floor which is also covered by butcher's broom and wood debris which are usually left lying where they fall in this reserve. As a consequence, apart from the first few days of the field campaign, soil temperature was lower than the air temperature with temperature excursion between day and night relatively low (1.7°C ± 0.8°C, data not shown), leading to an almost constant inversion in the lower layers below the canopy.

Vertical ozone concentrations measured at Bosco Fontana showed a relative peculiar course and three different regimes can be found. During the night, very stable stratification led to greater ozone concentrations in the outside canopy levels with relatively low differences between upper and lower measurements (3 ppb). More pronounced differences, greater than 10 ppb, were observed in forests by Karlsson et al. (2006) and Gerosa et al. (2005) but below canopy measurements in those studies were nearer to the ground, 3 m and 2 m respectively, while at Bosco Fontana the lowest measurement, excluding soil level one was at 16 m. Ozone concentrations measured at 0.15 m at Bosco Fontana showed during the night a much more similar reduction to Karlsson et al. (2006) and Gerosa et al. (2005). On the contrary, Launiainen et al. (2013) found a very low reduction of ozone concentrations also near the ground.

The heating of the crown enhanced the temperature gradient from 4:00 to 7:00 (2 K m^{-1}) and below canopy stability until the first hour after sunrise when the increase in friction velocity (Figure 6) was able

to mix the air also inside the forest leading to the second typical regime observed at Bosco Fontana, when the ozone concentrations from 16 to 41 m were almost equal; this condition was observed until noon.

After midday a third regime of ozone concentrations was observed with two different characteristics: at 32 m and at 24 m ozone concentrations were higher (3.7 ppb and 2.5 ppb respectively) than at 41 m, while 16 m ozone concentrations decreased. The explanation for the increase in ozone concentrations is not completely clear and one of the possible explanation lies in a local production, at canopy level, of ozone enhanced by the emission of very reactive VOCs as suggested, for instance, by Utiyama et al. (2003). The lifetime of these VOCs should be enough to reach the 32 m measuring point but not enough to influence 41 m measurements. The decrease in ozone concentrations at 16 m found a possible explanation in the effects of the thermal inversion, which got stronger in the afternoon, and in the start of the decrease of the friction velocity. A de-coupling of the atmosphere between the below and canopy layers seems a reasonable explanation, limiting the gas exchange between them. Below canopy ozone concentrations started to decrease because of NO emission from soil which destroy ozone by a gas-phase titration reaction (O_3+NO → O_2+NO_2). This phenomenon lasted for all the afternoon including from 16:00 also ozone concentrations at 24 m level, in agreement with what observed for the thermal inversion which got much steeper from 11 to 24 m. The maximum difference in ozone concentrations was observed at 17:30 and 41 m measurements were on average 10 ppb higher than 16 m ones. After 19:00, when a strong predominance of stable conditions was observed, the difference between the four levels decreased to nocturnal level.

Bosco Fontana forest acted as an ozone sink with rare upward fluxes (Figure 21); even if no indications of measurements above an oak-hornbeam were found in literature, the intensity of the fluxes was in the range of what has been observed for other ecosystems (Gerosa et al., 2009; Fares et al., 2014; Lamaud et al., 2002; Altimir et al., 2006, Launiainen et al., 2013; Zeller et al., 2001; Zapletal et al., 2011; Dorsey et al. 2004).

Only few studies measured ozone fluxes below canopy (Fares et al., 2014; Launiainen et al., 2013; Lamaud et al., 2002; Dorsey et al., 2004). In the first two papers below canopy fluxes were used for the parameterization of a deposition model rather than for the comprehension of in-canopy processes. Launiainen et al. (2013) found that the forest floor contributed up to 25–30% (nighttime) and 35–45% (daytime) to the total ozone deposition, while in our case was nearly 70% of the total deposition in the central hours of the day. Also, Dorsey et al. (2004) found that deposition to the forest floor was less than 40% of the total deposition to the forest, while Lamaud et al. (2002) found that below canopy fluxes were, on average, in two different field campaigns, 15 % and 45% of the above canopy fluxes. Dorsey et al. (2004) linked the below-canopy deposition to the NO soil emission, suggesting that nearly 60% of the emitted NO escaped the trunk space to react aloft. At Bosco Fontana a completely different situation

was observed: apart from the morning peak of NO (Figure 16) when concentrations ranged from 1 to 2 ppb, for the rest of the day they were less than 0.2 ppb and nearly constant at all the measuring levels; moreover, the decrease of the ozone concentrations at 0.15 m after midday, suggested a reaction of NO below canopy, which, following the vertical development of the thermal inversion started to affect the 16 m and the 24 m ozone concentrations with the consequent decrease of them in the afternoon.

Soil NO emissions were on average 76.8 ng N m^{-2} s^{-1}, similar to other published datasets (e.g. Butterbach-Bahl, 1997; Pilegaard et al. 1999) and likely the result of the large nitrogen deposition to this site from intense agricultural and industrial sources in the area. Twigg *et al*. (2015) measured a total dry deposition of 237 ng N m^{-2} s^{-1} averaged over this campaign, dominated by NH_3, but with important contributions also from NH_4NO_3 aerosol and HNO_3. By contrast NO and HONO made minor contributions.

played a significant role in the below canopy chemistry as already suggested by Kaplan et al. (1988) for a tropical forest and Mikkelsen et al. (2000) for a boreal forest. Pilegaard (2001) attributed 25 % of the ozone deposition to the reaction with NO. Rummel et al. (2002) measured NO fluxes at soil interface with a dynamic chamber system and by eddy-covariance at 7 m in the trunk space of a tropical forest. Nighttime measurements with these two systems were in good agreement during the night, with stable stratification and low turbulence, while during the day the eddy-covariance measurements were almost zero and soil fluxes still positive and similar to nighttime one. This situation seems very similar to what was observed in Bosco Fontana with a strong sink of ozone near the ground, caused by NO emission.

The application of a simple deposition model allowed to estimate a first partition of the ozone fluxes among the stomatal uptake, the reaction with NO and the reaction with VOCs and the destruction on surfaces. The bulk stomatal conductance was estimated from water vapor flux measurements, the reaction with NO was estimated from the difference in the NO flux measured above the canopy and soil and the reaction with isoprene was estimated from the flux of MVK/MACR measured above the canopy the remaining part was attributed to the destruction of ozone on surfaces and soil. More details about this procedure can be found in Nemitz et al. (2013). Results of this partition are show in Figure 23 where 40 % of the total ozone deposition was attribute to stomatal uptake, 30 % to the reaction with NO and only a minor part (<3 %) to reaction with VOCs. The large remaining part (27 %) was attributed to the destruction on soil or vegetated surfaces. The attribution of the reaction with NO seems sound (it is based on a simple stoichiometric reaction of NO with O_3) and comparable with what observed by Pilegaard et al. (2001) and Rummel et al. (2007). By contrast, the quantification of the stomatal pathway seems inconsistent with the flux gradient measured at Bosco Fontana: considering the difference between the ozone fluxes measured at 32 m and the ones measured below canopy at 16 m (Figure 24), only 35% was deposited to the crown layer, but this fraction should include the stomatal uptake but also the deposition to the vegetated surfaces of that layer. The attribution and the vertically resolved flux measurements can

only be resolved, if (a) a considerable stomatal sink also existed below the lowest flux measurement height and/or deposition to soil was a much more contributor to the un-attributed flux than deposition to the leaf cuticle.

Further investigations about the canopy chemistry should be performed: in fact the morning the ozone fluxes at 24 m, higher than the fluxes measured above, suggest that other reactions not considered here could be involved in a local production of ozone and a quick removal of it but no clear evidence of this fact were found.

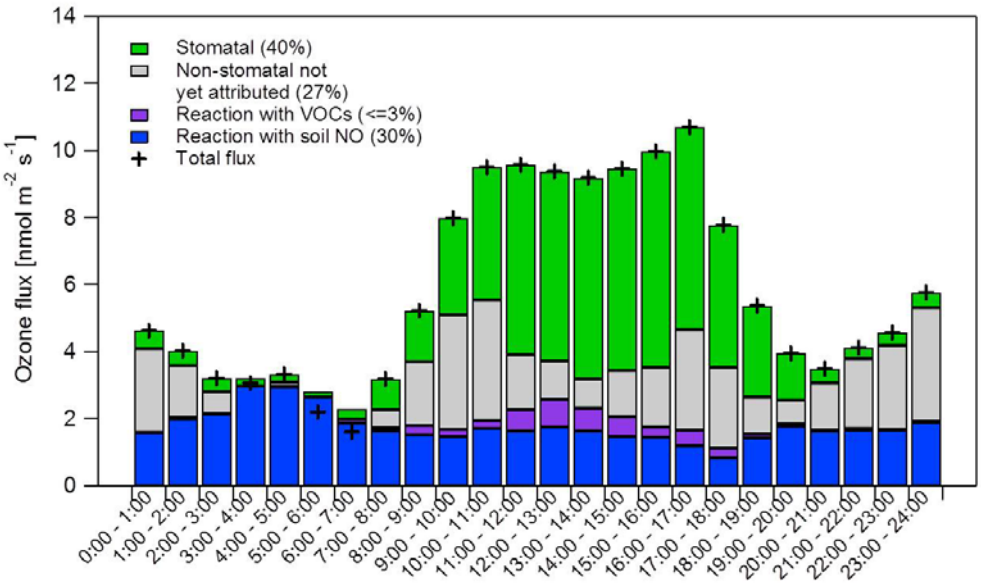

Figure 23. Attribution of the ozone flux measured above the canopy. The non-attributed flux reflects reactions with reactive VOCs other than isoprene as well as chemical destruction on surfaces of leaves and soil. At night the non-stomatal flux matches the destruction of NO below the measurement height within the uncertainty of the measurement

.

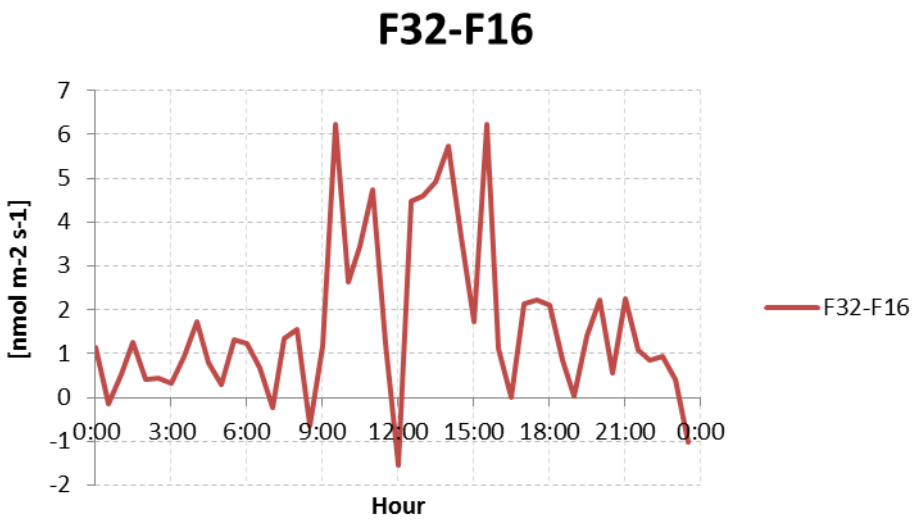

Figure 24. Average daily course of the difference between ozone fluxes above canopy (32 m) and below canopy (16 m)

5. Conclusions

Ozone flux measurements were made for the first time along a vertical profile with measurements above, inside and below the canopy. The higher level fluxes agreed closely and they were comparable with measurements on different forest ecosystems found in literature, although no measurements on oak-hornbeam forests like Bosco Fontana were run before.

The gas exchange between the forest and the atmosphere was influenced by a strong thermal inversion which affected the vertical concentrations of both nitrous oxide and ozone. In particular, the former increased only during stable stratification early in the morning while the latter showed a strong sink near the ground, due to NO emission. The combined effect of NO emission and of the thermal inversion led to ozone consumption which involved the entire space below canopy in the afternoon. The NO emissions from soil were estimated to account for the removal of one third of the total ozone deposition.

Canopy level measurements of ozone fluxes revealed a divergence of the fluxes, thus suggesting a possible local production, followed by a quick removal. Using a bulk resistance model, the stomatal flux was estimated to account for 40 % of the total deposition, whilst 30% of the O_3 flux was estimated to be controlled by reaction with soil NO emissions. Given that only 35% of the O_3 was lost in the crown space, it follows that (a) there were still stomatal sinks below the canopy, (b) deposition to leaf cuticle in crown space is small compared with deposition to soil and (c) most of the O_3-NO reaction occurs below the lowest measurement level, which is consistent with the NO concentration profile measurements.

Acknowledgements

This work was funded by the European FP7 project “ECLAIRE”. We are grateful to the Italian Corpo Forestale dello Stato for access to the measurement site.

References

Acton, W. J. F., Schallhart, S., Langford, B., Valach, A., Rantala, P., Fares, S., Carriero, G., Tillmann, R., Tomlinson, S. J., Dragosits, U., Gianelle, D., Hewitt, C. N., and Nemitz, E.: Canopy-scale flux measurements and bottom-up emission estimates of volatile organic compounds from a mixed oak and hornbeam forest in northern Italy, Atmos. Chem. Phys. Discuss., 15, 29213-29264, doi:10.5194/acpd-15-29213-2015, 2015.

Altimir, N., Kolari, P., Tuovinen, J.-P., Vesala, T., Back, J., Suni, T., Kulmala, M., Hari, P., 2006. Foliage surface ozone deposition: a role for surface moisture? Biogeosciences 3, 209–228.

Ashmore, M.R., 2005. Assessing the future global impacts of ozone on vegetation. Plant Cell and Environment. 28, 949–964.

Arya, S. Pal. 2001. *Introduction to micrometeorology*. San Diego: Academic Press.

Bellumè M., Maugeri M., Mazzucchelli E., 1998, Due secoli di osservazioni meteorologiche a Mantova, Edizioni CUSL, Milano (Italy), pp. 124

Butterbach-Bahl K, Gasche R., Breuer L., and Papen H., 1997. Fluxes of NO and N2O from temperate forest soils: impact of forest type, N deposition and of liming on the NO and N2O emissions, Nutr. Cycl. Agroecosyst., 48, 79-90.

Campanaro A., Hardersen S., Mason F., 2007, Piano di Gestione della Riserva Naturale e Sito Natura 2000 “Bosco della Fontana”. Quaderni Conservazione Habitat, 4. Cierre Edizioni, Verona (Italy), pp. 221

Cieslik S., Energy and ozone fluxes in the atmospheric surface layer observed in Southern Germany highlands, Atmospheric Environment, 1998, 32, 7, 1273

Cieslik, A. Labatut, Ozone and heat fluxes over a Mediterranean pseudosteppe, Atmospheric Environment, 1997, 31, *177*

Colbeck, I., Harrison, R.M., 1985. The photochemical pollution episode of 5–16 July 1983 in North-West England. Atmospheric Environment 19, 1921–1929.

Dizengremel, P., Jolivet, Y., Tuzet, A., Ranieri, A. and Le Thiec, D., Chapter 13 - Integrative Leaf-Level Phytotoxic Ozone Dose Assessment for Forest Risk Modelling, In: R. Matyssek, N. Clarke, P. Cudlin, T.N.

Mikkelsen, J.-P. Tuovinen, G. Wieser and E. Paoletti, Editor(s), Developments in Environmental Science, Elsevier, 2013, Volume 13, Pages 267-288, ISSN 1474-8177, ISBN 9780080983493,

Dorsey, J.R., Duyzer, J.H., Gallagher, M.W., Coe, H., Pilegaard, K., Weststrate, J.H.,Jensen, N.O., Walton, S., 2004. Oxidized nitrogen and ozone interaction withforests. I: Experimental observations and analysis of exchange with Douglas fir.Q. J. R. Meteorolog. Soc. 130, 1941–1955.

Ermel M., Oswald R., Mayer J.-C., Moravek A., Song G., Beck M., Meixner F. X., Trebs I., 2013. Preparation methods to optimize the performance of sensor discs for fast chemiluminescence ozone analyzers. Environmental Science and Technology 47, 1930-1936

Fares S., F. Savia, J. Muller, G. Matteucci, E. Paoletti, 2014 Simultaneous measurements of above and below canopy ozone fluxeshelp partitioning ozone deposition between its various sinks in a Mediterranean Oak Forest. Agricultural and Forest Meteorology 198–199 (2014) 181–191

Foken T. and Wichura B.,1996. Tools for quality assessment of surface-based flux measurements. Agricultural and Forest Meteorology 78, 83-105.

Gasche R., and Papen H., 1999. A 3-year continuous record of nitrogen trace gas fluxes from untreated and limed soil of a N-saturated spruce and beech forest ecosystem in Germany. 2. NO and NO2 fluxes, J. Geophys. Res., 104, 18505-18520

Gerosa, G., Vitale, M., Finco, A., Manes, F., Ballarin-Denti, A., Cieslik, S., 2005. Ozone uptake by an evergreen Mediterranean forest (Quercus ilex) in Italy. Part I: Micrometeorological flux measurements and flux partitioning. Atmospheric Environment 39, 3255–3266.

Gerosa, G., Finco, A.,Mereu, S., Vitale, M.,Manes, F., BallarinDenti, A., 2008. Comparison of seasonal variations of ozone exposure and fluxes in a Mediterranean Holm oak forest between the exceptionally dry 2003 and the following year. Environmental Pollution 157 (15), 1737–1744. doi:10.1016/j.envpol.2007.11.025.

Gerosa, G., Finco, A., Mereu, S., Marzuoli, R. & Ballarin Denti, A.. 2009. Interactions among vegetation and ozone, water and nitrogen fluxes in a coastal Mediterranean maquis ecoystem. Biogeosciences , 6, 1783-1798

Güsten H., Heinrich G., 1996. On-line measurements of ozone surface fluxes: Part I. Methodology and instrumentation. Atmospheric Environment 6, 897-909.

Karlsson P.E., Hansson M., Hoglund H.-O., Pleijel H., 2005. Ozone concentration gradients and wind conditions in Norway spruce (Picea abies) forests in Sweden. Atmospheric Environment 40 (2006) 1610–1618

Kaplan, W. A., Wofsy, S. C., Keller, M. and Da Costa, J. M.: 1988, 'Emission of NO and deposition of O3 in a tropical forest system', *J. Geophys. Res.* **93**(D2), 1389–1395.

Lamaud, E., Carrara, A.,Brunet, Y., Lopez, A., Druilhet, A., 2002. Ozone fluxes above and within a pine forest canopy in dry and wet conditions. Atmos. Environ. 36,77–88

Langford B., W. Acton, C. Ammann, A. Valach, and E. Nemitz, 2015. Eddy-covariance data with low signal-to-noise ratio: time-lag determination, uncertainties and limit of detection. Atmos. Meas. Tech. Discuss., 8, 2913-2955,

Launiainen, S., Canopy processes, fluxes and microclimate in a pine forest. Report series in aerosol science N:o 117 (2011)

Launiainen, S., Katul, G.G., Gronholm, T., Vesala, T., 2013. Partitioning ozone fluxes between canopy and forest floor by measurements and a multi-layer model. Agric. For. Meteorol. 173, 85–99.

Lee, X., Massman, W., and Law, B., 2004. Handbook of Micrometeorology: A Guide for Surface Flux Measurements and Analysis. Kluwer Academic Publisher, Dordrecht.

Longo L., 2004. Clima, In: Mason F. (ed.). Dinamica di una foresta della Pianura Padana. Bosco della Fontana. Seconda edizione con Linee di gestione forestale. Rapporti Scientifici 1. Centro Nazionale Biodiversità Forestale Verona - Bosco della Fontana. Arcari Editore, Mantova (Italy), pp. 16-17

Marzuoli,R., Gerosa, G., Desotgiu, R., Bussotti, F., Ballarin-Denti, A., 2008. Ozone fluxes and foliar injury development in the ozone-sensitive poplar clone Oxford (Populus maximowiczii · Populus berolinensis): a dose–response analysis. Tree Physiology 29, 67–76 doi:10.1093/treephys/tpn012

Massman, W.J., 1992. A surface energy balance method for partitioning evapotranspiration data into plant and soil components for a surface with partial canopy cover. Water Resources Research 28, 1723–1732.

Matyssek, R., Innes, J.L., 1999. Ozone—a risk factor for trees and forests in Europe? Water Air Soil Pollution. 116, 199–226.

Matyssek, R., Sandermann, H., Wieser, G., Booker, F., Cieslik, S., Musselman, R., Ernst, D., 2008. The challenge of making ozone risk assessment for forest trees more mechanistic. Environmental Pollution 156, 567–582.

Matyssek, R., Wieser, G., Calfapietra, C., de Vries, W., Dizengremel, P., Ernst, D., Jolivet, Y., Mikkelsen, T.T., Mohren, G.M.J., Le Thiec, D., Tuovinen, J.P., Weatherall, A., Paoletti, E., 2012.

Forests under climate change and air pollution: gaps in understanding and future directions for research. Environmental Polluion. 160, 57–65.

McMillen, R. T.: 1988, 'An Eddy Correlation Technique with Extended Applicability to Non-Simple Terrain', Boundary-Layer Meteorol. 43, 231–245.

Mikkelsen T.N., H. Ro-Poulsen, M.F. Hovmand, N.O. Jensen, K. Pilegaard, A.H. Egeløv, Five-year measurements of ozone fluxes to a Danish Norway spruce canopy, Atmospheric Environment, Volume 38, Issue 15, May 2004, Pages 2361-2371, ISSN 1352-2310, http://dx.doi.org/10.1016/j.atmosenv.2003.12.036.

Monteith, J. L. and Unsworth, M. H.: Principles of environmental physics, 291 pp., Edward Arnold, London, 2014.

Nemitz E., B. Langford, C.F. Di Marco, M. Coyle, C. Braban, M. Twigg, G. Gerosa, A. Finco, A. Valach, J. Acton3, B. Loubet, S. Schallart, R. Gasche, E. Diaz-Pines, S. Fares, J. Westerlund, Å. Hallquist, C. Gritsch, S. Zechmeister-Boltenstern and M.A. Sutton. Quantifying Chemical Interactions in a Forest Canopy – First Results from the ÉCLAIRE Campaign at Bosco Fontana, Po Valley. Accent plus symposium, Urbino 2013

Neumann, H.H. and Den Hartog, G. (1985). Eddy correlation measurements of atmospheric fluxes of ozone, sulphur, and particulates during the Champaign Intercomparison Study. Journal of Geophysical Research 90: doi: 10.1029/JD090iD01p02097. issn: 0148-0227.

Padro J., Summary of ozone dry deposition velocity measurements and model estimates over vineyard, cotton, grass and deciduous forest in summer, Atmospheric Environment, Volume 30, Issue 13, July 1996, Pages 2363-2369, ISSN 1352-2310, http://dx.doi.org/10.1016/1352-2310(95)00352-5.

Pilegaard, K., Hummelshøj, P. and Jensen, N. O.: 1999, 'Nitric oxide emission from a Norway spruce forest floor', *J. Geophys. Res., D* **104**, 3433–3445.

Pilegaard K., 2001. Air–soil exchange of NO, NO2 and O3 in forests. *Water, Air, and Soil Pollution: Focus* **1:** 79–88.

Rosenkranz P., Brüggemann N., Papen H., Xu Z., Seufert G., and Butterbach-Bahl K., 2006. Biogeosciences, 3, 121-133.

Rummel, U., Ammann, C., Kirkman, G. A., Moura, M. A. L., Foken, T., Andreae, M. O., Meixner, F. X., 2007. Seasonal variation of ozone deposition to a tropical rain forest in southwest Amazonia. Atmos. Chem. Phys. 7, 5415–5435

Rummel, U., Ammann, C., Gut, A., Meixner, F. X., and Andreae, M. O.: Eddy covariance measurements of nitric oxide flux within an Amazonian rainforest, J. Geophys. Res., 107(D20), 8050, doi:10.1029/2001JD000520, 2002.

Twigg, M.M., Di Marco, C.F., Langford, B., Loubet, B., Gerosa, G., Finco, A., Sutton, M.A., Nemitz, E.: Controls of reactive nitrogen fluxes and gas-aerosol interactions above a semi-natural forest in the Po Valley, Italy. Atmos. Chem. Phys. Discuss. [in preparation]

Utiyama, M., Fukuyama, T., Maruo, Y.Y., Ichino, T., Izumi, K., Hara, H., Takano, K., Suzuki, H., Aoki, M., 2004. Formation and deposition of ozone in a red pine forest. Water, Air, & Soil Pollution 151, 53–70.

Vickers D. and L. Mahrt, 1997: Quality Control and Flux Sampling Problems for Tower and Aircraft Data. J. Atmos. Oceanic Technol., 14, 512–526.

Webb, E. K., Pearman, G. I., and Leuning, R., 1980. Correction of flux measurements for density effects due to heat and water vapour transfer, Q. J. Roy. Meteor. Soc., 106, 85–100

Wesely, M.L., 1983. Turbulent transport of ozone to surfaces common in the eastern half of the United States. Advances in Environmental Science and Technology 12, 345–370.

Wilczak, J. M., Oncley , S. P., Sage, S. A.: 2001, ‘Sonic anemometer tilt correction algorithms’, Bound.-Layer Meteorol. 99, 127-150.

Wu X., Brüggemann N., Gasche R., Shen Z., Wolf B., Butterbach-Bahl K., 2010. Glob Biogeochem Cycl, 24, GB2012, doi: 10.1029/2009GB003616

Zapletal, M., Cudlín, P., Chroust, P., Urban, O., Pokorný, R., Edwards-Jonásová, M., Czerný, R., Janou_s, D., Taufarová, T., Ve_ce_ra, Z., Miku_ska, P., Paoletti, E., 2011. Ozone flux over a Norway spruce forest and correlation with net ecosystem production. Environmental Pollution 159, 1024e1034.

Zona D., B. Gioli, S. Fares, T. De Groote, K. Pilegaard, A. Ibrom, R. Ceulemans, Environmental controls on ozone fluxes in a poplar plantation in Western Europe, Environmental Pollution, Volume 184, January 2014, Pages 201-210, ISSN 0269-7491, http://dx.doi.org/10.1016/j.envpol.2013.08.032.